AFRL-VS-HA-TR-2005-1053

Seismic Energy Generation and Partitioning into Various Regional Phases from Different Seismic Sources in the Middle East Region

Yefim Gitterman
Vladimir Pinsky

Geophysical Institute of Israel
P.O.B. 182, Lod
71100 Israel

13 March 2005

Annual Report

AIR FORCE RESEARCH LABORATORY
Space Vehicles Directorate
29 Randolph Rd
AIR FORCE MATERIEL COMMAND
Hanscom AFB, MA 01731-3010

This technical report has been reviewed and is approved for publication.

AFRL-VS-HA-TR-2005-1053

/signed/

ROBERT J. RAISTRICK
Contract Manager

/signed/

ROBERT BELAND, Chief
Battlespace Surveillance Innovation Center

This report has been reviewed by the ESC Public Affairs Office (PA) and is releasable to the National Technical Information Service (NTIS).

Qualified requestors may obtain additional copies form the Defense Technical Information Center (DTIC). All others should apply to the National Technical Information Service.

If your address has changed, if you with to be removed from the mailing list, or if the addressee is no longer employed by your organization, please notify AFRL/VSIM, 29 Randolph Rd., Hanscom AFB, MA 01731-3010. This will assist us in maintaining a current mailing list.

Do not return copies of this report unless contractual obligations or notices on a specific document require that it be returned.

Using Government drawings, specifications, or other data included in this document for any purpose other than Government procurement does not in any way obligate the U.S. Government. The fact that the Government formulated or supplied the drawings, specifications, or other data does not license the holder or any other person or corporation; or convey any rights or permission to manufacture, use, or sell any patented invention that may relate to them.

This report is published in the interest of scientific and technical information exchange and its publication does not constitute the Government's approval or disapproval of its ideas or findings.

REPORT DOCUMENTATION PAGE

Form Approved
OMB No. 0704-0188

1. REPORT DATE (DD-MM-YYYY)	2. REPORT TYPE	3. DATES COVERED (From - To)
23-03-2005	Technical (Annual)	1 Jan 2004 to 31 Dec 2004

4. TITLE AND SUBTITLE
Seismic Energy Generation and Partitioning into Various Regional Phases from Different Seismic Sources in the Middle East Region

5a. CONTRACT NUMBER
F19628-03-C-0124

5b. GRANT NUMBER

5c. PROGRAM ELEMENT NUMBER
62601F

6. AUTHOR(S)
Yefim Gitterman and Vladimir Pinsky

5d. PROJECT NUMBER
5101

5e. TASK NUMBER
SM

5f. WORK UNIT NUMBER
A1

7. PERFORMING ORGANIZATION NAME(S) AND ADDRESS(ES)

Geophysical Institute of Israel
P.O.B. 182, Lod
71100 Israel

8. PERFORMING ORGANIZATION REPORT NUMBER 542/123/05(2)

9. SPONSORING / MONITORING AGENCY NAME(S) AND ADDRESS(ES)
AIR FORCE RESEARCH LABORATORY
29 Randolph Rd
Hanscom AFB, MA 01731-3010

Contract Manager : R. Raistrick AFRL/VSBYE

10. SPONSOR/MONITOR'S ACRONYM(S)
AFRL

11. SPONSOR/MONITOR'S REPORT NUMBER(S)
AFRL-VS-HA-TR-2005-1053

12. DISTRIBUTION / AVAILABILITY STATEMENT
Approved for public release; distribution is unlimited

13. SUPPLEMENTARY NOTES

14. ABSTRACT

An event database was created to study empirical features of seismic energy generation from explosions, and how this energy is partitioned between P and S waves. The explosions selected present a broad variety of design features and geological settings. A number of experimental single-fired explosions were conducted and numerous observations were acquired from the near-source zone to near-regional distances by stations in Israel and Jordan. From regional observations of the Sayarim charge-weight series, significant seismic strength was achieved in spite of a dry alluvium media, commonly considered as low-coupling material, and shallow burial depth. Existing software was modified and new programs were developed. As a case study analysis the computer procedures were applied to the Sayarim shots. Results show dependencies of S/P maximum amplitude and energy ratios on distance and yield. Source scaling estimations show similar yield scaling parameters (0.87-0.93) for different phases, in close agreement with the constants for explosions in Nevada and Wyoming. Application of the spectral ratio technique to data collected for some explosions provided estimates of the corner frequency-charge relation and the equivalent yield of a partially detonated explosion. The analysis will be continued for other events from the dataset selected and new planned experimental shots to validate the results obtained.

15. SUBJECT TERMS
Seismic energy generation Experimental single-fired explosions S/P amplitude and energy ratios Source scaling Spectral ratio

16. SECURITY CLASSIFICATION OF:			17. LIMITATION OF ABSTRACT	18. NUMBER OF PAGES	19a. NAME OF RESPONSIBLE PERSON
a. REPORT	b. ABSTRACT	c. THIS PAGE			Robert J. Raistrick
UNCLASSIFIED	UNCLASSIFIED	UNCLASSIFIED	SAR	46	19b. TELEPHONE NUMBER (include area code) 781-377-3726

Standard Form 298 (Rev. 8-98)
Prescribed by ANSI Std. 239.18

SUMMARY

During the first year of the project, numerous data were collected to study empirical features of seismic energy generation (especially for S waves from explosions) for different seismic sources; and how this energy is partitioned between P, S and surface waves, in specific geological conditions and tectonic settings of the Middle East. The sources include experimental explosions, military detonations, and routine quarry blasts, for which Ground Truth information (GT0) and blast design parameters were collected. A number of experimental explosions were conducted in this project (Sayarim and Mehola experiments), others in a MERC (US AID program) project (October 2004) (on-land detonations in single holes, and 2 underwater explosions [UWE] in the Dead Sea). Some earthquakes were included in the database, for comparative waveform analysis.

An extensive dataset was collected from the selected seismic events recorded by short-period and broadband stations in Israel and Jordan, providing different manifestations of S-waves at regional distances (up to 390 km for the largest events). We analyzed quantification of the source coupling for contained (with different scaled depth), single-fired, chemical experimental explosions observed at regional stations. A charge-weight explosion series (0.3, 2 and 32.5 tons of ANFO) was conducted in Sayarim Valley, Israel (June 2004), under the auspices of this research and a MERC project, providing data for yield-dependent analysis of regional waveforms. Good records were obtained for the series in the near-source area by accelerometers at distances 100-500 m, and numerous portable and network seismic SP and BB stations, up to ~400 km. PGA values and BB station EIL amplitudes (r~30 km) are well matched with a power law dependence on yield. Similar power law scaling parameters were determined for each of the dominant regional phases: P (0.93), S (0.87) and Rg (0.93). Significant seismic strength was achieved (M_L~2 for 2 ton and M_L~3 for 32.5 ton) in spite of emplacement of the explosives in dry alluvium and a shallow burial depth, commonly considered as low-coupling factors. We started to estimate and analyze S/P maximum amplitude and energy ratios for selected events in different time and frequency bands, against distance and charge weight.

Existing GII software for visualization and preliminary processing of accelerograms and seismograms was modified and adapted for the project goals, including SEISPECT (analysis of

spectra and spectral ratios), and AIST (waveform analysis of different data formats). Appropriate software for the S/P amplitude and energy ratio estimation was developed.

SUMMARY ii

1. COLLECTION OF DATA AND GROUND TRUTH INFORMATION 1

1.1. Conducting experimental explosions and collection of observations. 1

1.1.1. Sayarim charge weight series 1

1.1.2. Mehola and MERC experimental shots. 4

1.2. Large controlled land blasts and selected earthquakes 5

2. DEVELOPMENT AND MODIFICATION OF SOFTWARE FOR ANALYSIS OF DATA OBTAINED 7

2.1. Visualization and preliminary processing 7

2.2. Estimation of seismic energy generation and partitioning between P and S waves 9

2.2.1. S/P Maximum Amplitude Ratio in different Frequency bands. 9

2.2.2. S/P Energy Ratio in fixed frequency range 9

3. DATA PROCESSING AND ANALYSIS OF RECORDINGS FOR DATASET SELECTED 11

3.1. Near-source observations by 3C accelerometers and portable seismic stations 11

3.1.1. Accelerometer waveform analysis and estimation of subsurface velocities. 11

3.1.2. Estimated PGA attenuation scaling. 15

3.1.3. Seismograms at close distances 20

3.2. Network SP and BB stations 22

3.2.1. Analysis of waveforms and manifestation of different regional phases 22

3.2.2. Source Scaling estimations. 26

3.2.3. S/P maximum amplitude ratios in different frequency bands 35

3.2.4. Estimating energy partitioning for observed phases. 37

4. CONCLUSIONS 42

5. REFERENCES 43

Figures

Figure **Page**

Figure 1. Location of seismic events selected and seismic stations for observations. On the insert two profiles of ~800 IRIS SP sensors are shown, deployed during the single-shot explosions in October 2004 (including the MERC project). 2

Figure 2. Graphic interface of SEISPECT program for an ETNA accelerogram from the Sayarim explosion S2 (2 tons). 7

Figure 3. AIST interface showing regional waveforms of the largest Sayarim explosion (S3) recorded at SP stations of ISN (format *.dta), JSN (*.gse) and BB station AMZI (format SAC). 8

Figure 4. Location and configuration of explosions and near-source observations for Sayarim (left) and Mehola (right) experiments..... 11

Figure 5. Acceleration waveforms for single-hole shot S2 (left) and multiple-hole explosion S3 (right) of the Sayarim experiment. The modified SEISPECT software was used for visualization and analysis of the accelerograms obtained..... 12

Figure 6. Comparison of accelerograms (uncorrected) of the two Mehola explosions recorded at ~450 m. When plotted in the absolute scale waveforms from Ex1A are not seen due to very weak signal (left), then the relative scale is used (right)..... 13

Figure 7. Velocity transform (bottom) of acceleration (top) emphasizes the S-wave for Mehola explosion Ex1A (station ACC6, hypocentral distance is 235 m). 14

Figure 8. Travel times for direct P and S waves measured on accelerograms of Mehola explosions, providing a rough estimation of subsurface velocity structure..... 15

Figure 9. Estimation of PGA vector attenuation parameters for Sayarim explosions..... 16

Figure 10. Dependence of peak accelerations on charge for vertical component and vector for Sayarim shots. For ExS3 an effective equivalent charge is between 3 and 25 tons. 16

Figure 11. Attenuation of vector peak accelerations vs scaled distance. 17

Figure 12. Attenuation of vertical peak accelerations vs scaled distance for different explosions and geological settings..... 18

Figure 13. Vector attenuation with distance for experimental shots of similar charge weight. 18

Figure 14. Spectral ratios of the two Mehola shots for different wave phases observed at remote accelerometer acc4 (r~450 m). 20

Figure 15. Seismograms of the Mehola explosions at 3-C portable station #1 (r~3 km). Note that scales for left (Ex1A) and right (Ex1B) plots are different. 21

Figure 16. Spectra of Mehola shots at portable Station #3 (r~10 km). 21

Figure 17. Seismogram of the large 32.5 ton shot recorded by the IMS array AS049..... 22

Figure 18. Sample of distinct S-waves for two explosions of similar design (charge 1 ton in a single hole), observed at ISN stations (vertical components). 23

Figure 19. Different S-wave manifestation for an explosion and an earthquake located close to each other (~6 km) in the Dead Sea Transform zone. 25

Figure 20. Illustration of the procedure using spectral ratios for estimating corner frequency of single-fired explosions. 26

Figure 21. Seismograms (relative scale) recorded at CSS station (80 sps, r~10 km) for the pair of Cyprus shots (a), and smoothed spectra of the whole signal (8 sec) (b). 27

Figure 22. 3C seismogram of the large Cyprus explosion at CSS station (a) and smoothed amplitude spectra of different phases for both explosions on the vertical component (b). 28

Figure 23. Spectral ratios for different wave phases at 3 components of BB station CSS 29

Figure 24. Empirical corner frequency-yield relation based on data from single-fired contained explosions in Cyprus and Wyoming. 30

Figure 25. Spectral ratio for the two Mehola shots at portable station St.1 (EW - about transversal). A time window of 2 sec was used, including P and S waves. 31

Figure 26. Spectral ratio for the two Mehola shots on the vertical component of ISN station HMDT. A time window of 20 sec was used, including the whole signal. 32

Figure 27. Seismograms of Sayarim explosions at EIL (vertical) in relative (left) and absolute (right) scale. 33

Figure 28. 3C seismogram at EIL BB station of the largest Sayarim Ex.S3. Three regional phases can be identified. 33

Figure 29. Peak amplitude (vertical component) source scaling for different phases at local distances 34

Figure 30. S/P maximum amplitude ratios vs distance for observations at different SP ISN stations from single-fired explosions in the Sayarim area. 35

Figure 31. S/P maximum amplitude ratios vs charge averaged for different ISN stations for Sayarim explosions (top); mean and standard deviation estimations for the medium filter (3-6Hz) (bottom). Number of processing stations (n) is also shown. 36

Figure 32. Amplitudes (m/sec) versus time (sec) for six 3C stations (3 BB and 3 SP stations) (shot ExS3). Vertical lines mark time intervals for energy computation. 38

Figure 33. Energy partitioning between P, S and Rg (surface waves) for the six 3C stations as computed in the time intervals shown in Figure 32 (shot ExS3). 39

Figure 34. Amplitudes (m/sec) versus time (sec) for sixteen vertical channels of the BB and SP stations (explosion ExS3). Vertical lines indicate time intervals for energy computation. 40

Figure 35. Energy partitioning between P, S and Rg (surface waves) for sixteen 3C vertical stations as computed in the time intervals shown in Figure 34 (shot ExS3). 41

Tables

Table **Page**

Table 1. Parameters of Sayarim experimental explosions..... 3
Table 2. Estimated equivalent (single borehole) charges and scaled depth for Sayarim series. 3
Table 3. Parameters of Mehola and MERC shots and selected earthquakes (Oct. 2004). 4
Table 4. Parameters of selected large land blasts with Ground Truth information. 6
Table 5. Scaling coefficients for the three explosions and Exp1A charge estimation. 19
Table 6. Estimated source scaling parameters in Equation (8). 34

1. COLLECTION OF DATA AND GROUND TRUTH INFORMATION

During the first year of the project an initial dataset was collected to study empirical features of seismic energy generation (especially for S waves from explosions) for different seismic sources; and how this energy is partitioned between P and S waves, in specific geological conditions and tectonic settings of the Middle East. The sources include 15 experimental explosions (mostly in single boreholes), 2 strong routine quarry blasts and a military detonation, where Ground Truth information (GT0) and blast design parameters were collected. Two earthquakes that occurred during the experimental observation period were also included for the comparative waveform analysis.

1.1. Conducting experimental explosions and collection of observations.

During 2004 GII conducted a number of experimental explosions in Israel for the project.

1.1.1. Sayarim charge weight series.

A series of three experimental explosions of varying charge (ANFO explosive) was conducted in the Sayarim Valley near Eilat, Israel (Figure 1, Table 1). The largest single-fired shot of 32.5 tons, in 11 large-diameter (60-70 cm) boreholes of ~20 m depth, was designed as a large-scale on-land seismic calibration explosion as part of the MERC project TA-MOU-99-M18-035 of the U.S. AID, for the purpose of improving regional velocity models for calculating travel times of seismic waves to regional seismic stations and calibration of IMS station AS49 at Mt. Meron. Two smaller explosions of 0.3 ton and 2 tons were conducted at the same site, in single boreholes of the same depth and diameter, thus providing (together with the calibration shot) a series for yield-dependent analysis of regional waveforms. The large diameter hole contributed to a smaller linear size of the cylinder charges, approaching near-spherical configuration, and promoted more concentration of explosives for the largest shot (only 11 holes for 32.5 tons). Geologically the area is a graben filled by Quaternary alluvial conglomerates, underlain by consolidated limestone, chalk and chert rocks, thus large diameter boreholes could be drilled. A seismic refraction survey provided P-velocity estimates of Vp~1600-1700 m/sec in the upper layers of soft sediments (where the charges were placed), and Vp~2000 m/sec, for consolidated rocks, evidently chalk, that prevented drilling to depth greater than 20-21 m.

A number of portable instruments were installed during the explosion series: five ETNA accelerometers in the near-source zone at distances 0.1-2 km, and four 3-component seismic

stations at distances of 20-100 km to the North. Good waveform records were collected from strong-motion instruments and numerous portable and network short-period and broad-band seismic stations in Israel and Jordan (Figure 1).

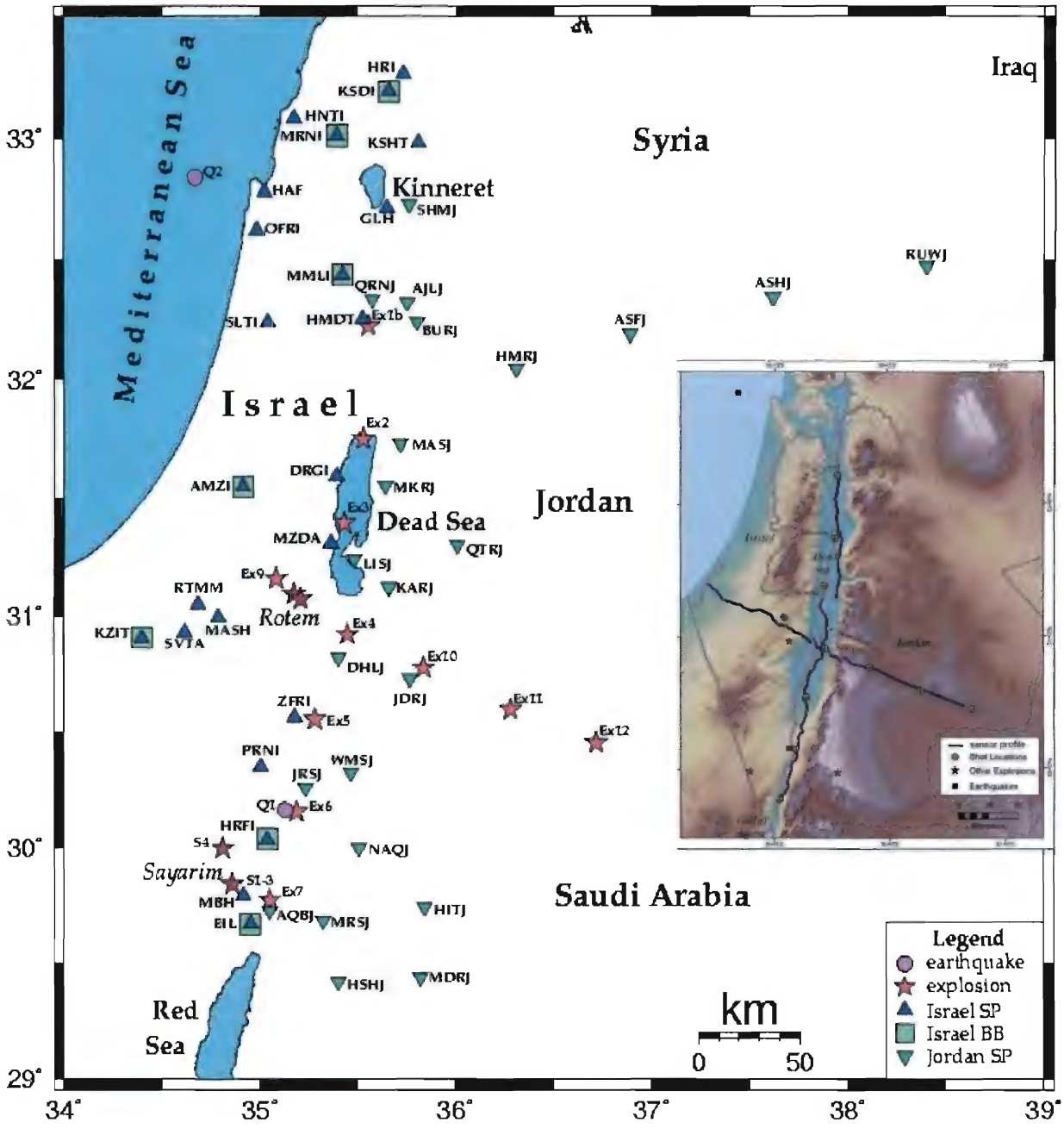

Figure 1. Location of seismic events selected and seismic stations for observations. On the insert two profiles of ~800 IRIS SP sensors are shown, deployed during the single-shot explosions in October 2004 (including the MERC project).

As expected, for the largest explosion clear seismic signals were observed at the remote IMS array AS049 at Mt. Meron (r~350 km). All of the explosion series was recorded successfully at IMS BB station EIL and small-aperture sesmic array EILESA near Eilat (r~20 km), providing a basis for source-scaling analysis (see Chapter 3.2.2). For comparison with data obtained from other observations, the ANFO charges were converted to TNT equivalent (Table 2) according to the IME TNT Equivalence Calculator (http://www.ime.org/calculator/index.html) and ISEE Blasters' Handbook (17^{th} ed.). We also calculated the scaled (burial) depth, an important parameter of underground explosions that characterizes seismic energy generation and surface effects (Table 2):

$$\hat{h}\ (m/kg^{1/3}) = H(m)/(W, kg)^{1/3} = 0.01\ H(m)/(W, kT)^{1/3} \quad (1)$$

where H – charge depth, W – single charge weight in kg or kT (kilotons).

Table 1. Parameters of Sayarim experimental explosions.

Ex. No	Date	Coordinates		Origin Time, GMT	M_L	ANFO charge, kg	Hole depth, m	No. of holes
		Lat. Lon.	Local X, Y, km					
S1	13.06.04	29.84334 34.85866	136.031 -82.729	12:20:01.192	-	300	20	1
S2	15.06.04	29.84244 34.85860	136.025 -82.829	11:49:39.349	2	2000	20	1
S3	15.06.04	29.84188 34.85851	136.017 -82.890	13:00:01.493	3	32500	17-20.5	11

Table 2. Estimated equivalent (single borehole) charges and scaled depth for Sayarim series.

Ex. No	Single charge W1, kg	TNT equiv.,kg	Charge(center) depth, m	Scaled depth,m/kg$^{1/3}$	Explosion containment, cratering effect
S1	300 (ANFO) +20 (booster)	262	19.5	3.05	fully contained, no crater
S2	2000 (ANFO) +20	1635	16.5	1.40	partially contained, symmetric round crater was created (radius ~13-14m, depth ~1.5 m)
S3	3000 (ANFO) +20	2442 (total 26860)	15	1.11	poorly contained, a number of non-symmetric craters were created and merged into irregular strongly deformed surface

The large-diameter hole depth at this site did not prevent rock blowout and energy losses into the air, and cratering. From regional observations, significant seismic strength was achieved (M_L~2 for S2 and M_L~3 for S3) in spite of the non-consolidated sediment medium - dry alluvium,

considered commonly as a low-coupling material (e.g. U.S. Congress, 1988), and shallow burial depth that caused poor containment.

1.1.2. Mehola and MERC experimental shots.

A number of experimental explosions were conducted in October 2004 (Table 3). Two shots were performed for this project (Mehola experiment, Ex1A&1B). Others were part of the MERC (US AID) project TA-MOU-01-M21-012: a) land detonations in single holes, in dry or water-saturated media, in different geological and tectonic settings in Israel and Jordan, on both sides of the Dead Sea Transform zone, b) two underwater shots in the Dead Sea. IRIS blast boxes provided detonations at pre-determined times. Ground Truth (GT0) information was collected for all the explosions (Table 3), with broad variety of blast design parameters, charge geometry, geological settings, and emplacement media (different rocks, dry and water-filled and underwater shots).

Table 3. Parameters of Mehola and MERC shots and selected earthquakes (Oct. 2004).

Event	Day	GMT	Country	Lat.°	Long.°	Elev., m (depth, km)	Location	Design	Mag. M_L
Ex12	Oct 20	10:10	Jordan	30.45359	36.71731	1008	N.W.Inab	1 ton	-
Ex1A		**11:15**	**Israel**	**32.22269**	**35.55644**	**-300**	**Mehola area**	**3 ton (?), h=25m**	**-**
Ex1B		**12:15**	**Israel**					**3 ton, h=35m**	**2.4**
Ex11		13:01	Jordan	30.59726	36.2808	962	N. of Jafr	1 ton	<0.5
Ex10		15:00	Jordan	30.77727	35.83613	1033	Jurf Darawish	1 ton	<1
Ex3		15:05	Israel	31.3949	35.43104	-417	DeadSea (South)	0.75 ton TNT at H=50m	3.2
Ex7	Oct 21	08:00	Jordan	29.7736	35.04994	63	East Timna	1 ton	1.95
Ex9		08:15	Israel	31.15981	35.0822	515	Aroe'r	1 ton ANFO d=70cm, h=23m	1.9
Ex6		10:00	Jordan	30.15717	35.18869	189	QaSaidin	1 ton	~1.6
Ex5		12:00	Jordan	30.55579	35.28107	13	E.Zofar	1 ton cratering and collapse	1.4
Ex4		14:00	Jordan	30.92097	35.44713	-305	Fifa		?
Ex2		15:05	Israel	31.74982	35.5270	-417	DeadSea (North)	0.75 ton TNT at H=50m	3.1
Earthquakes									
Q1	Oct20	11:16:57.1		30.164	35.13	9	Arava Valley		2.1
Q2	Oct21	14:17:52.3		32.844	34.67	9	Mediterranean		2.0

Explosion 1A produced anomalously small amplitudes relative to Ex1B, which was of similar charge weight. Field observations, video-recordings and close-in ground motion records from the

anomalous shot suggest that the explosives did not completely detonate, resulting in reduced amplitudes (see below, Chapters 3.1.2 and 3.2.2). All the explosions (except the very weak Ex12 in Jordan) were recorded by ISN (Israel Seismic Network) stations. BB station data (IMS and CNF) were also collected, when signals were observed. Two of the explosions (Dead Sea underwater shots, Ex.2&3) were recorded by the Jordanian Seismic Network (as triggered events; data supplied by Dr. A.-Q. Amrat of NRA, Jordan). Data from the deployment of ~800 IRIS 24-bit SP seismometers along two long refraction profiles (see Figure 1), intended to investigate the crust along the Dead Sea rift zone (the MERC project), recording the explosions and earthquakes shown in Table 3, will be collected later.

1.2. Large controlled land blasts and selected earthquakes

We also collected GT information and records for three large land quarry/military blasts conducted in 2004 (see Table 4, Figure 1). A specific feature of these sources is unusually large seismic energy released, shown by high local magnitude M_L values estimated from Israel network observations. Rotem quarry blast R2 of 15 tons (ANFO) in several dozen holes with many delays produced a seismic event with magnitude 2.9 that is very close in magnitude to the Sayarim experiment large simultaneous explosion S3 of 32.5 ton (ANFO) in 11 holes (located ~120 km to the South) that yielded magnitude ~3.0 (see Chapter 1.1.1.). Likewise, the military shot S4 of ~10 ton of TNT, intended to destroy out-dated ammunition, indented very slightly into the ground and open to the air, produced a significant magnitude 2.5, and clear seismic signals are observed up to 160 km, as well as very strong acoustic waves. Some earthquakes, recorded in the same period and close to the explosion sources, were included in the project database for comparative waveform analysis (Table 3).

Table 4. Parameters of selected large land blasts with Ground Truth information.

Event	Date, Site	Origin time, GMT (estimated from ISN records)	M_L	Local coordinates X, Y, km		Total charge, kg	Delay msec	No. of del.	No. of holes	Blast pattern
				GPS Meas	Estim. ISN					
R1	25.04.04 Rotem phosphate quarry	9:15:18.5	2.7	-	166.52 55.810	13278 ANFO	25	6	211	hole depth 3-7m spacing 6x7m diameter ~7" stemming 50%
R2	22.07.04 Rotem quarry	9:54:46.9	2.9	-	169.8 53.51	~15000 ANFO	?	23	?	?
S4	07.06.04 Sayarim area	15:06:28.4	2.5	131.3 -66.1	131.6 -65.5	~10000 TNT	0	Surface explosion in 0.5-1m deep trench in Sayarim military range - to destroy out-date-ammunition		

A portable 3C seismic station was installed at ~15 km from the Rotem blasts, and good quality data were obtained.

2. DEVELOPMENT AND MODIFICATION OF SOFTWARE FOR ANALYSIS OF DATA OBTAINED

For the processing and analysis of data obtained in the project we utilized software packages developed in GII that were modified and improved to fit the objectives of the project.

2.1. Visualization and preliminary processing

For visualization and preliminary processing of near-source observations of ETNA accelerometers and portable seismic stations we utilized the GII newly-developed software SEISPECT (by N. Perelman). The program, created in the PC-Windows environment using the MATLAB platform, was modified to read ETNA source records in format *.evt, and compute FFT spectra and spectral ratios (see Figure 2).

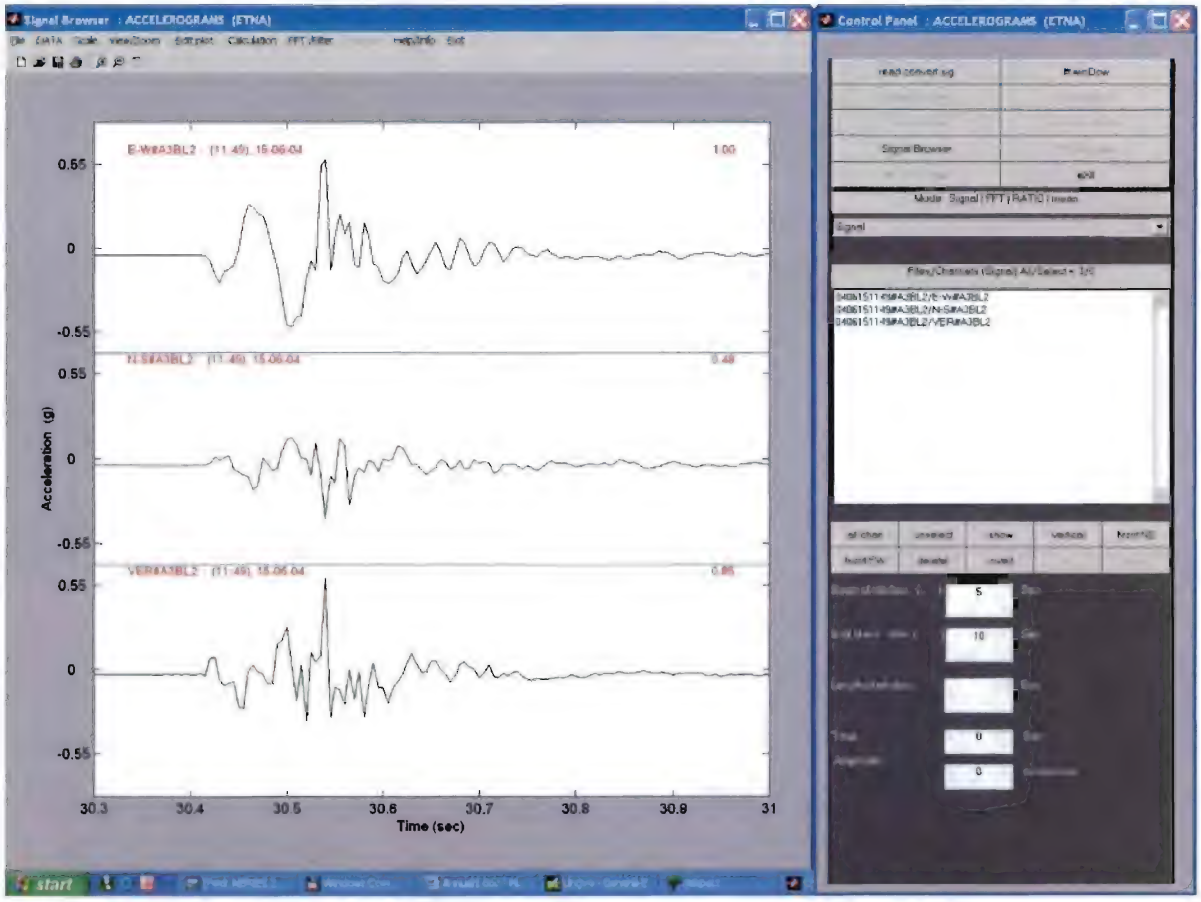

Figure 2. Graphic interface of SEISPECT program for an ETNA accelerogram from the Sayarim explosion S2 (2 tons).

For visualization and preliminary processing of all data collected from seismic stations with different formats, we utilized the newly-developed software AIST (by A. Polozov and Dr. V. Pinsky, GII). The program was modified to read data from short-period stations of Israel (format *.dta) and Jordanian (format *.gse) networks, and broad-band stations (formats SEED and SAC), and provide joint visualization and analysis of waveforms from a single event in differently formatted records (Figure 3):

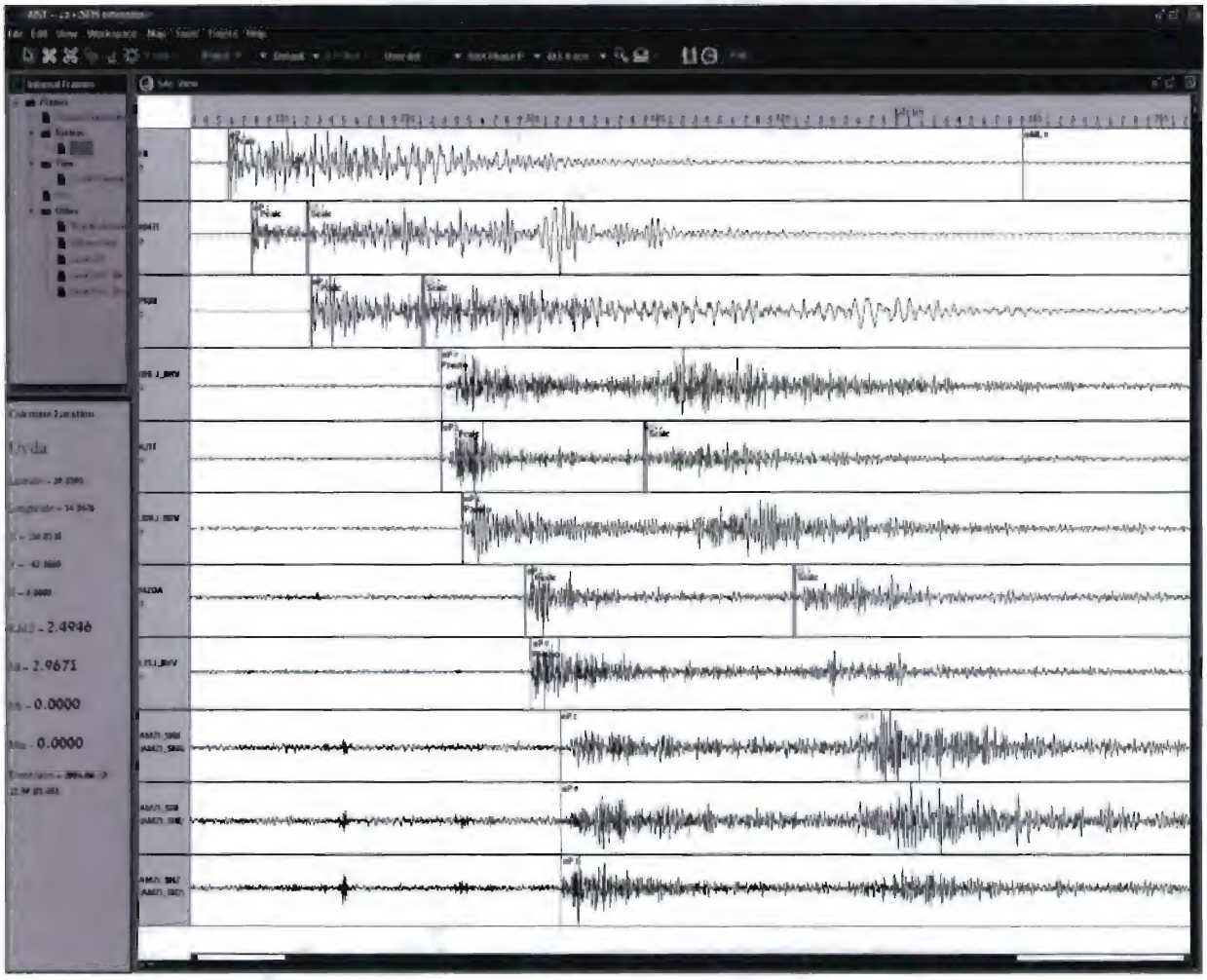

Figure 3. AIST interface showing regional waveforms of the largest Sayarim explosion (S3) recorded at SP stations of ISN (format *.dta), JSN (*.gse) and BB station AMZI (format SAC).

2.2. Estimation of seismic energy generation and partitioning between P and S waves

2.2.1. S/P Maximum Amplitude Ratio in different Frequency bands.

For the analysis of S-waves generation from explosions a new procedure of calculating S/P maximum amplitude ratio in different frequency bands was developed and incorporated in a new DSE software package (by N. Perelman). The DSE (Discrimination of Seismic Events) software is intended for identification of explosions and earthquakes recorded by local stations, and has been applied to local seismic events by J. Kurpan as partial fulfillment of her Master thesis (Kurpan et al., 2004). The DSE is based on the SEISPECT program, and is designed and programmed in the PC-Windows environment and the MATLAB-platform. The recording frequency range for short-period Israel stations (0.5-12Hz) was divided into three bands (0.5-3Hz; 3-6Hz; 6-9Hz), that together with the whole (broad) range (0.5-12Hz, i.e., unfiltered signal) were used for calculation and analysis.

Measured arrivals of P and S waves from ISN bulletin phase files are used to estimate time windows for the maximum amplitude calculation. The P-wave window is selected between the first arrivals of P and S-waves. The S-wave window is taken as equal to the P-window length if it is less than 3 seconds, a time window 3 seconds is used for both wave types when the distance from source to the station r<100km, and 5 seconds, when r>100 km. A theoretical arrival time for P or S-waves is calculated from a local velocity model if one of them is absent in the phase file for a station. The average maximum amplitude S/P ratio and standard deviation are also calculated for each filter.

2.2.2. S/P Energy Ratio in fixed frequency range

A number of programs and scripts were developed for calculation of seismic energy of different regional phases observed on seismograms (by Dr. V. Pinsky). The processing procedure includes the following elements:

1) Data for each seismic event is in "dta" format (short-period ISN stations) and SAC format (BB stations). Based on the software AIST interface the data is analysed and filtered in a specified frequency band.

2) Using the AIST interface data (velocity) files of an event (with instrument response removed) are transferred from the original formats to special ASCII format files for each channel.

3) Further data processing is carried out by a shell script using the list of channels of the 3C stations "CICLION3C" and "CICLION1C" for vertical stations.

4) The "CICLION3C" script filters each of the channels in the given frequency band.

5) Then 3C channels of the stations are selected to compute a vector trace:

$$G(t)=[X(t)^2+Y(t)^2+Z(t)^2]^{0.5} \quad (1)$$

for each station in the list.

6) For each station the distance is computed using Cartesian coordinates of the source Xe, Ye, and station Xs, Ys:

$$D= [(Xe-Xs)^2+(Ye-Ys)^2]^{0.5} \quad (2)$$

7) Travel times for the first P and S wave arrivals $\boldsymbol{TT_p}$ and $\boldsymbol{TT_s}$ are computed according to the local 1D layered velocity model (used in GII for routine location) by the "TTCOMP" procedure of A. Shapira.

8) From the calculated travel times and known origin time T_0 (for the Ground Truth explosions) the theoretical arrival times TA_p and TA_s are computed for each trace: $\boldsymbol{TA=T_0+TT}$, and constitute the left limit of the analyzed windows for P and S phases on seismograms.

9) The right limit is determined by the length of the window WL, which in this study was chosen as 2 sec for P and S phases.

10) The surface Rayleigh waves window starts 0.5 sec after the S wave window and ends at the S wave double lapse time $\boldsymbol{TE= T_0+2TT_s}$.

11) The whole signal window starts at $\boldsymbol{TA_p}$ and ends at $\boldsymbol{TE}$.

12) Seismic wave energy in each of the specified windows – the whole signal window AW, P window PW, S window SW and Rayleigh waves window RW - is calculated:

$$E = \sum_{t \in W} G(t)^2 \quad (3)$$

13) Energy in the specified windows are presented in the table of results as percent (%) of energy $\boldsymbol{E}$ computed in the whole signal window AW, and in appropriate plots.

3. DATA PROCESSING AND ANALYSIS OF RECORDINGS FOR DATASET SELECTED

3.1. Near-source observations by 3C accelerometers and portable seismic stations

During two explosion experiments conducted for the project in 2004, we deployed a number of ETNA accelerometers and 3C short-period seismic stations (see Figure 4), to study S-wave manifestation at near-source distances.

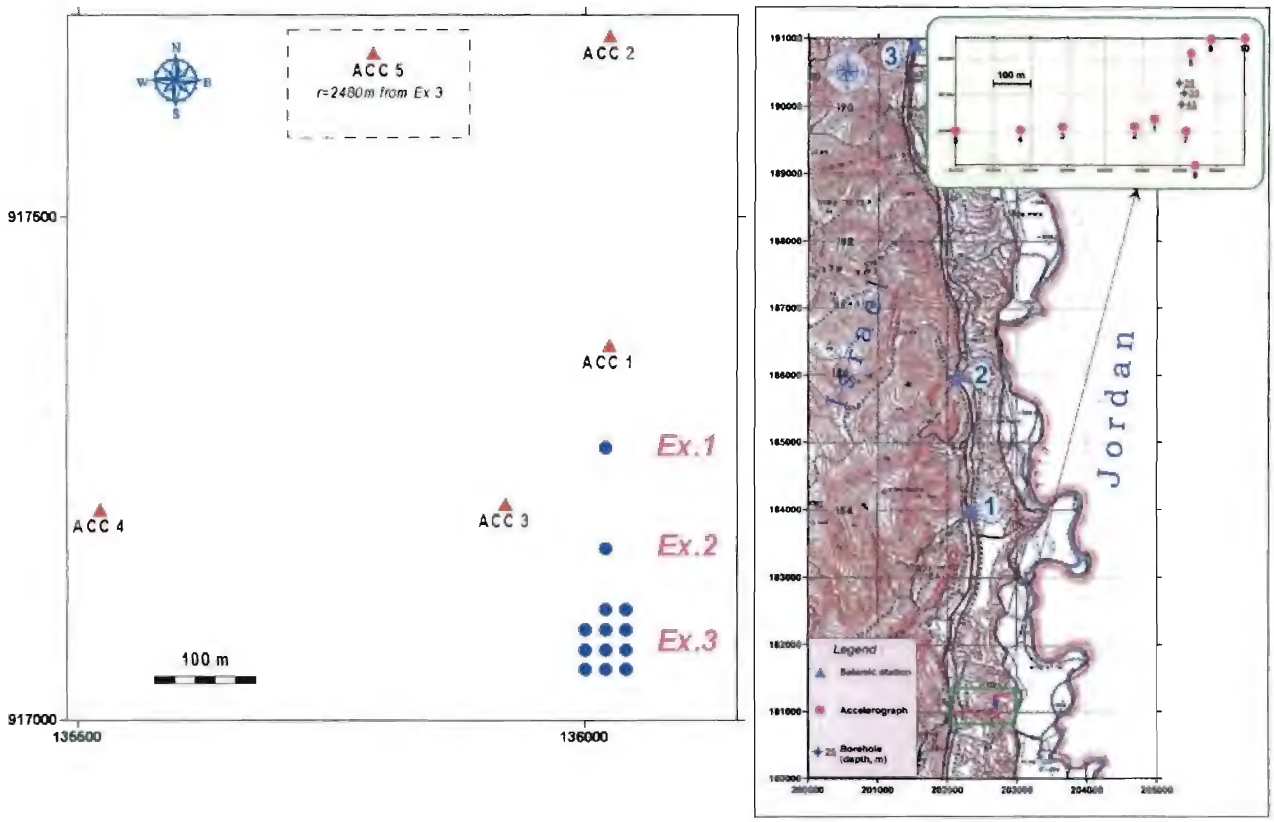

Figure 4. Location and configuration of explosions and near-source observations for Sayarim (left) and Mehola (right) experiments.

3.1.1. Accelerometer waveform analysis and estimation of subsurface velocities.

Seismic source complexity for Sayarim explosion S3, conducted in 11 boreholes, was observed at the closest accelerometer, with two wave groups (separated by ~0.2 sec) found on all three components; the first group is like the signal from the single-hole shot S2 (Figure 5). The accelerogram is similar to near-field strong-motion data from Lyaur explosions with delayed detonations in multiple rows (Negmatullaev et al., 1999). There were no delays for explosion S3, all borehole charges were detonated simultaneously, but due to hole spacing, the distance

difference from the closest and remotest charges to station ACC3 was ~60-70 m, and an appropriate time shift could reach ~0.2 sec for S-wave velocity ~300-350 m/s.

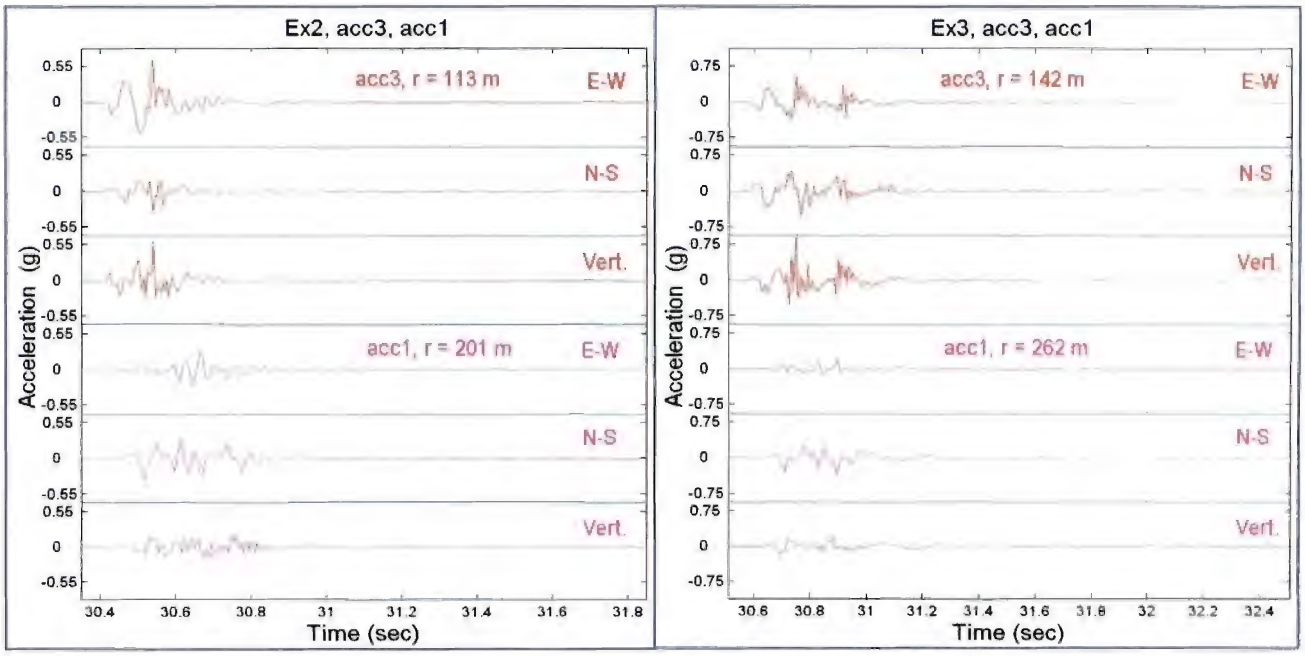

Figure 5. Acceleration waveforms for a single-hole shot S2 (left) and multiple-hole explosion S3 (right) of the Sayarim experiment. The modified SEISPECT software was used for visualization and analysis of the accelerograms obtained.

Comparison of amplitudes and waveforms for the two Mehola explosions at the same station (see an accelerogram sample in Figure 6) shows that the second explosion Ex1B was much stronger than Ex1A, confirming visual and sensory observations during the experiment. PGA (Peak Ground Accelerations) more than 2g were registered for Ex1B. The ratio of PGA values for the two explosions at the same station varies from 10 to 40 for different stations and components. As mentioned before we suggest that for Ex1A the explosives did not completely detonate. Different detonation features and water conditions in the boreholes may have caused the distinct S-wave manifestation for the two explosions (Figure 6), rather than different hole depths: S-wave amplitudes for the weak Ex1A are comparable with R-waves, whereas for the strong Ex1B S-waves are negligible.

Data analysis for the Mehola experiment showed that S-waves are more pronounced on velocigrams, than on accelerograms (see an example in Figure 7), and demonstrate higher amplitudes and energy than P-waves at very short distances, where direct seismic waves are dominant. We note that velocigrams are also more appropriate for estimations of induced seismic energy and wave propagation velocities in the source vicinity. Preliminary estimates (Figures 7, 8) showed ~1370 m/s for P-waves, and ~ 300 m/s for S-waves, corresponding satisfactorily to the geological setting of the area, containing subsurface Quaternary alluvium deposits.

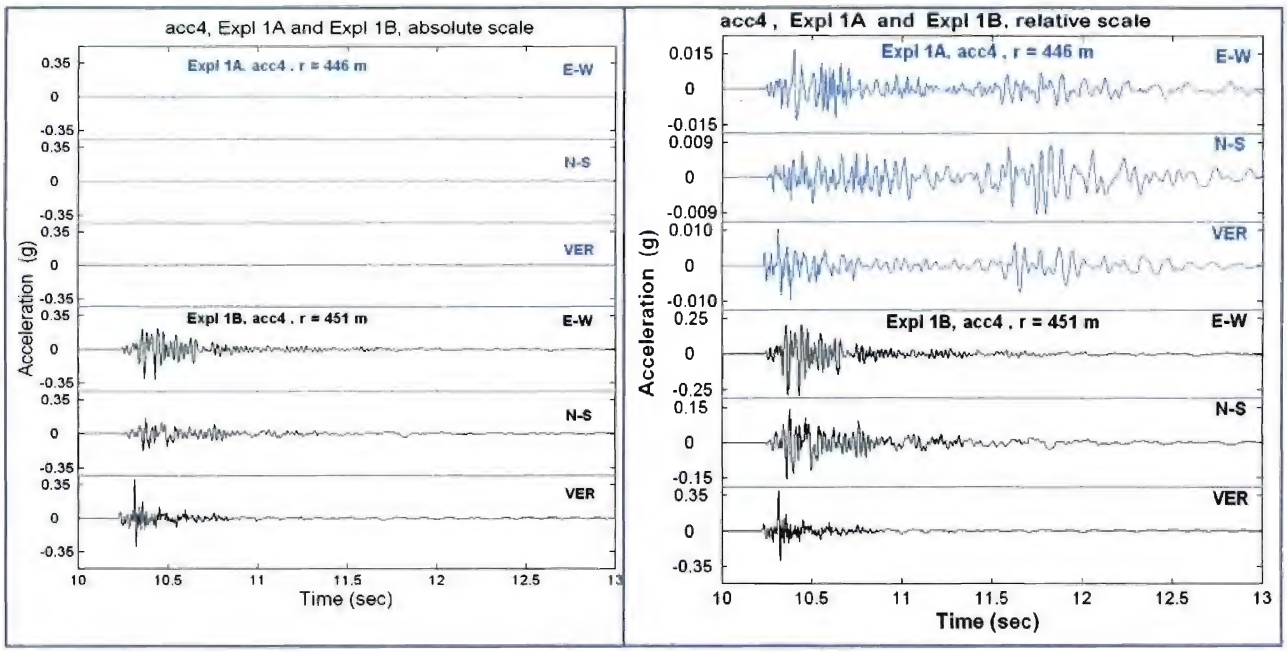

Figure 6. Comparison of accelerograms (uncorrected) of the two Mehola explosions recorded at ~450 m. When plotted in absolute scale waveforms from Ex1A are not seen due to very weak signal (left), then the relative scale is used (right).

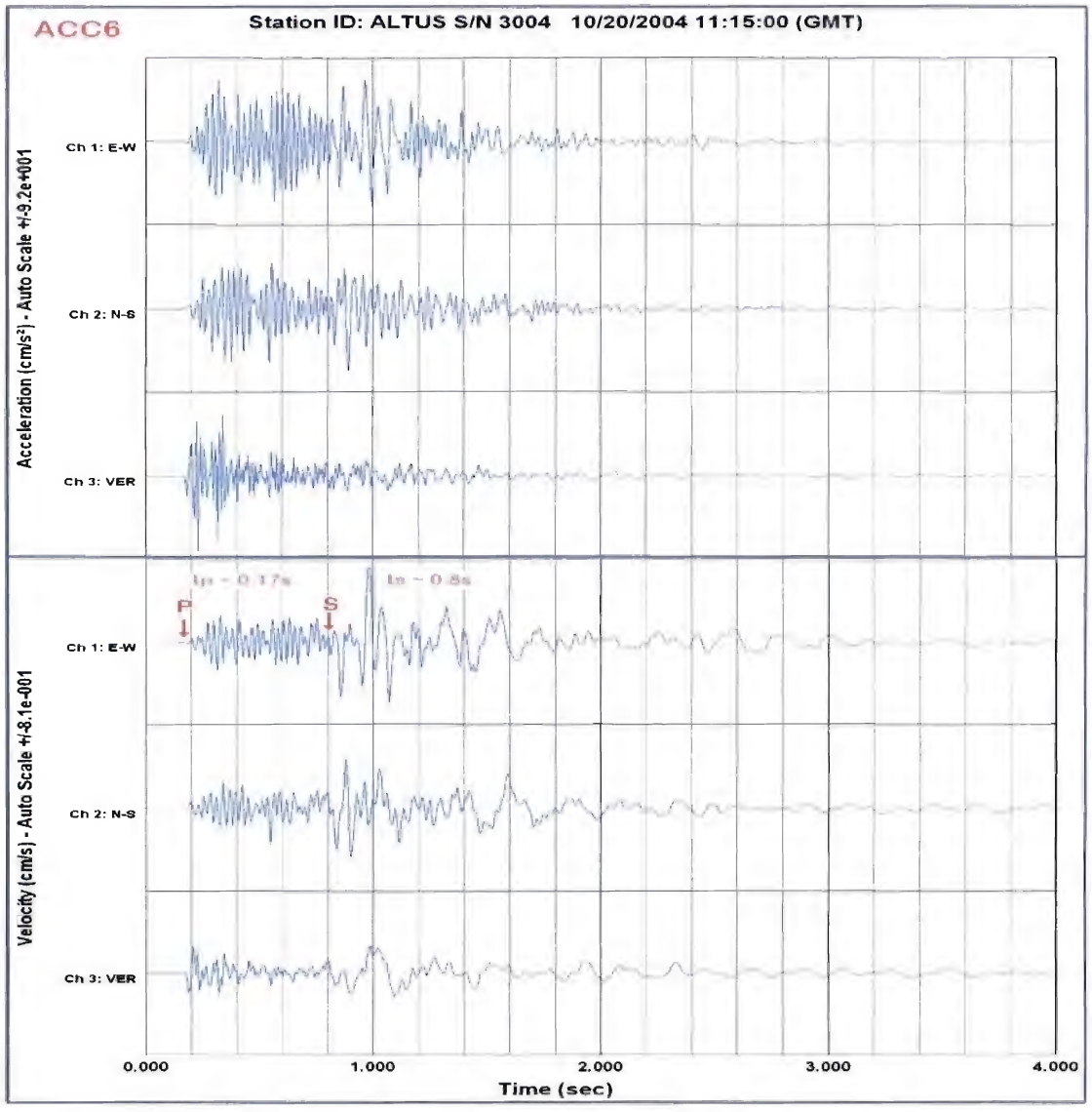

Figure 7. Velocity transform (bottom) of acceleration (top) emphasizes the S-wave for Mehola explosion Ex1A (station ACC6, hypocentral distance is 235 m).

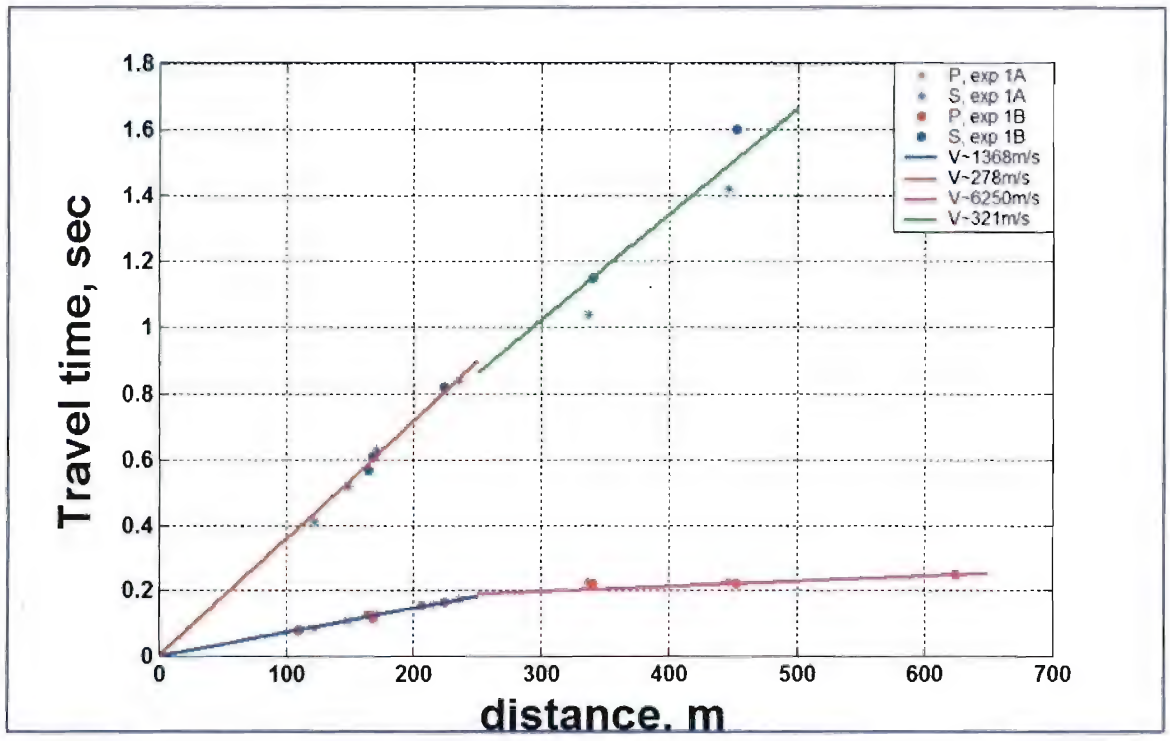

Figure 8. Travel times for direct P and S waves measured on accelerograms of Mehola explosions, providing a rough estimation of subsurface velocity structure.

3.1.2. Estimated PGA attenuation scaling.

We calculated Peak Ground Accelerations (PGA) measured by ETNA accelerometers for the three components (E-W, N-S and vertical) and the maximum vector as:

- $PGA_{vector} = (PGA_{EW}^2 + PGA_{NS}^2 + PGA_{vert}^2)^{1/2}$ (4)

We estimated attenuation with distance for the vertical component and the vector. The data are fit with the power relation:

$$PGA_{(cm/s\^2)} = a*r_{(m)}^{b} \quad (5)$$

Similar attenuation parameters b_i were obtained for all three explosions (see Figure 9); therefore we applied an average fixed value $b = -1.74$ for the 3 lines to estimate the scale coefficients a_i, used for yield scaling parameters estimation (Figure 10). The results show that in the near-source zone peak accelerations (both vertical and vector) increase approximately as the square root of the charge weight. For ExS3 both single hole charge W_1 and the total charge W_Σ were used for the analysis because only close holes contribute substantially to PGA values at very short distances and the effective equivalent charge is between W_1 and W_Σ.

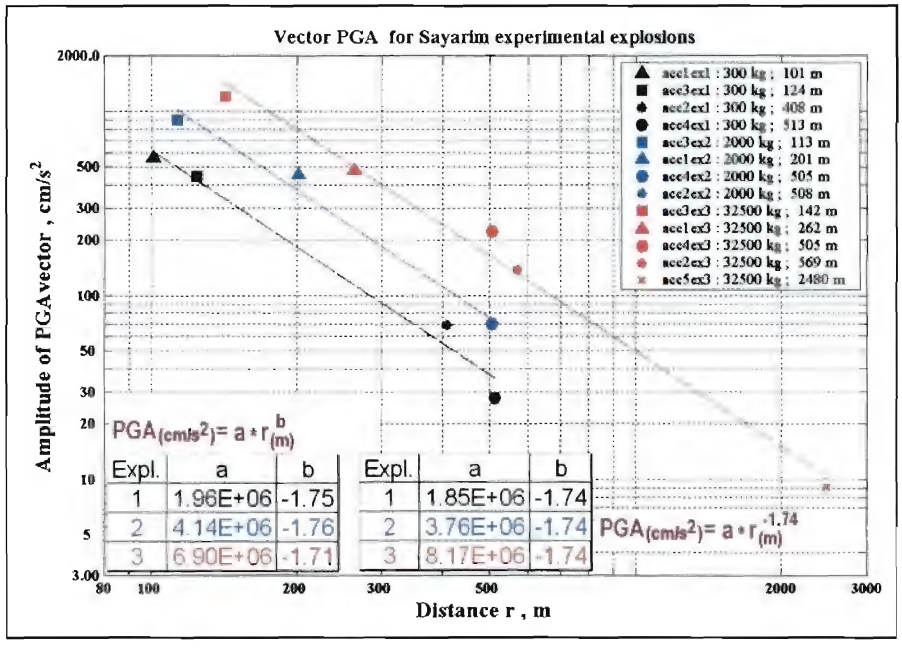

Figure 9. Estimation of PGA vector attenuation parameters for Sayarim explosions.

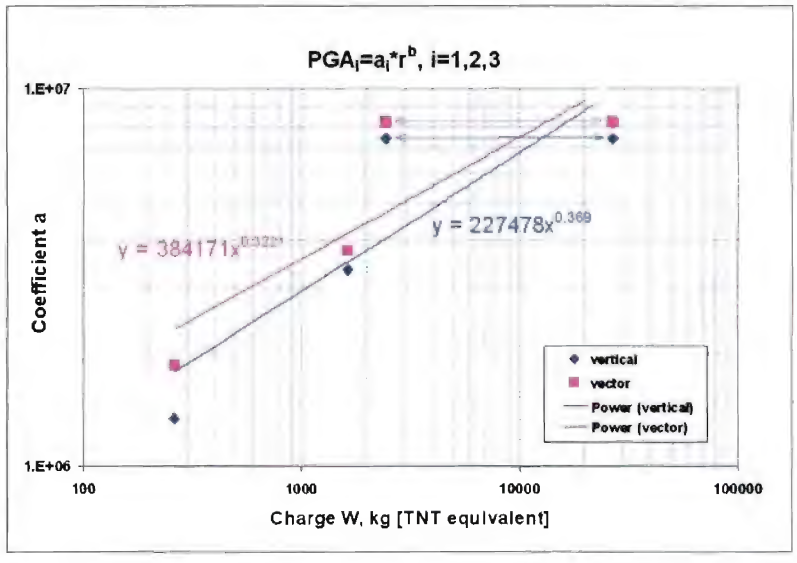

Figure 10. Dependence of peak accelerations on charge for vertical component and vector for Sayarim shots. For ExS3 an effective equivalent charge is between 3 (single hole charge) and 25 (the total charge) tons.

Using the scaled distance $R=r/W^{1/3}$ reduced but did not remove the difference between the three attenuation lines (Figure 11). To compute R for the multiple-hole explosion ExS3, we used the closest hole charge (TNT equivalent, Table 2), instead of the total weight of the explosive ANFO. The divergence for the three Sayarim shots relates to different scaled depth (Table 2) for

ExS1 and ExS2, and contribution of more than one hole charge to peak amplitudes for the large multiple-hole ExS3 compared to the single-hole ExS1 and ExS2.

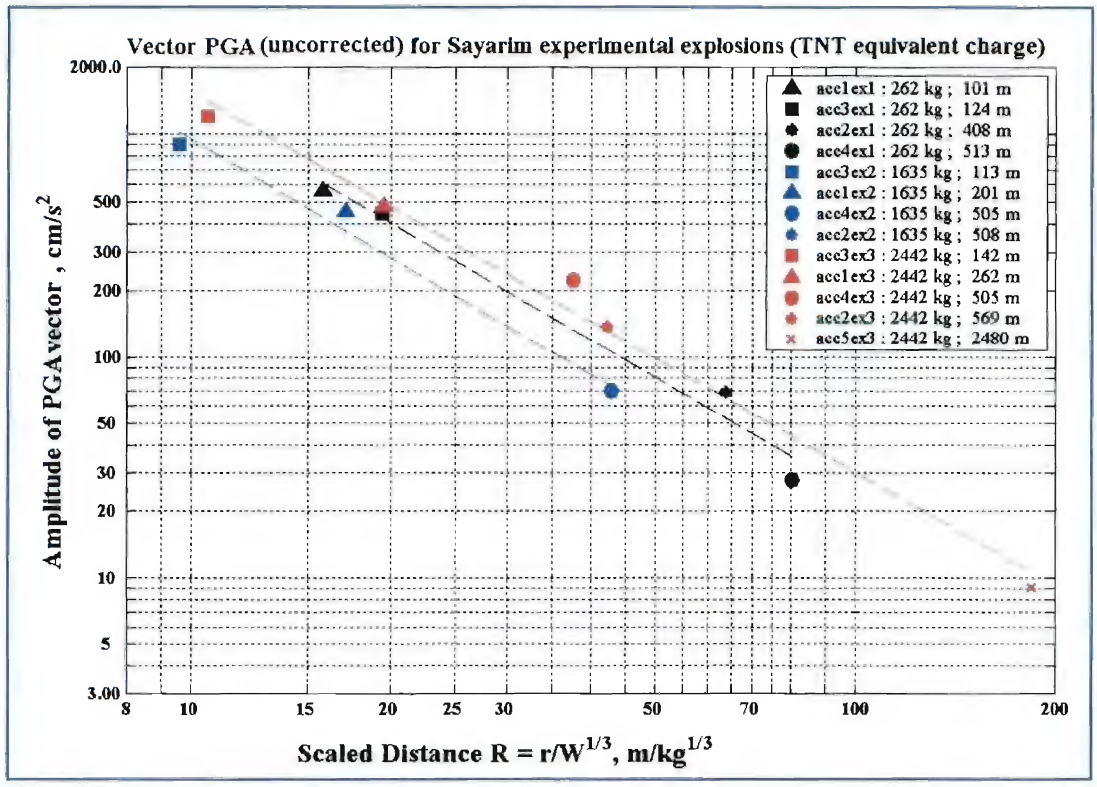

Figure 11. Attenuation of vector peak accelerations vs scaled distance.

The amplitudes for the Sayarim shots in dry alluvium/conglomerates are higher than values for the Lyaur explosions in loess (Negmatullaev et al., 1999), and lower than for explosions in consolidated sediments (Rotem) and hard rocks (Cyprus) (Figure 12), that GII conducted recently in for another project (see Gitterman and Pinsky, 2004).

The same estimates of the power relation parameters (in Eq. 5) were obtained for the pair of Mehola explosions. Similar values of the parameters b_i were found for both explosions, close to the average value of power factor $b = -1.74$ for Sayarim explosions (see Figure 13). Therefore we applied this fixed value to the Mehola pair and compared to the Sayarim single-hole shot ExS2 of similar charge weight to estimate the scaling coefficients a_i for each explosion, and then estimated yield for Ex1A (Figure 13).

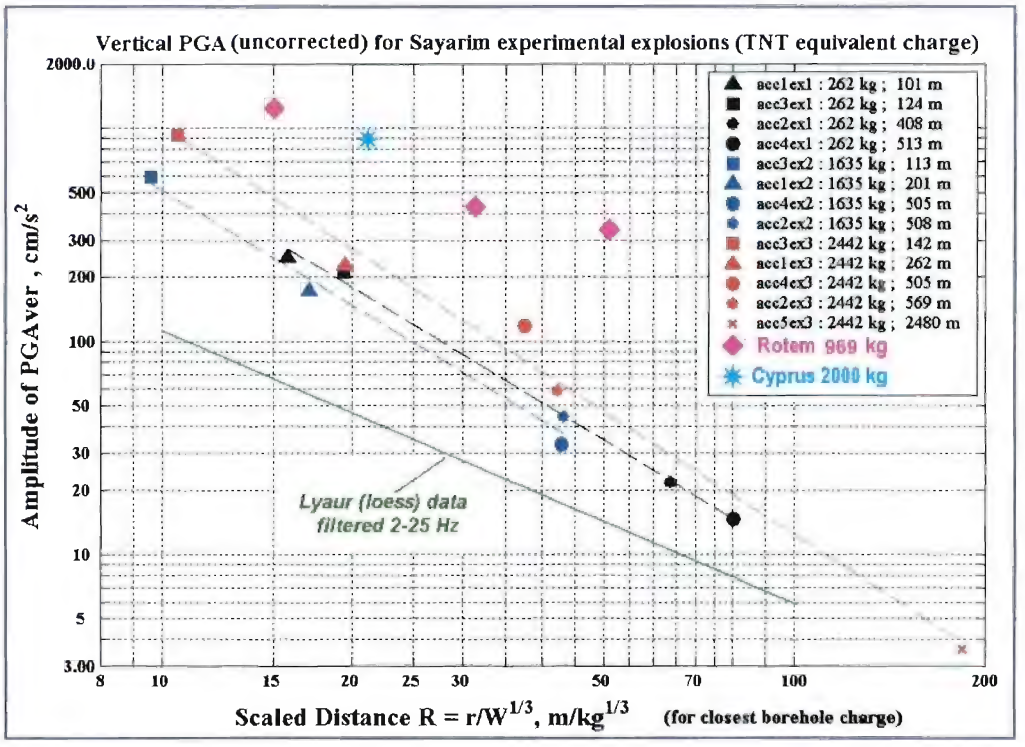

Figure 12. Attenuation of vertical peak accelerations vs scaled distance for different explosions and geological settings.

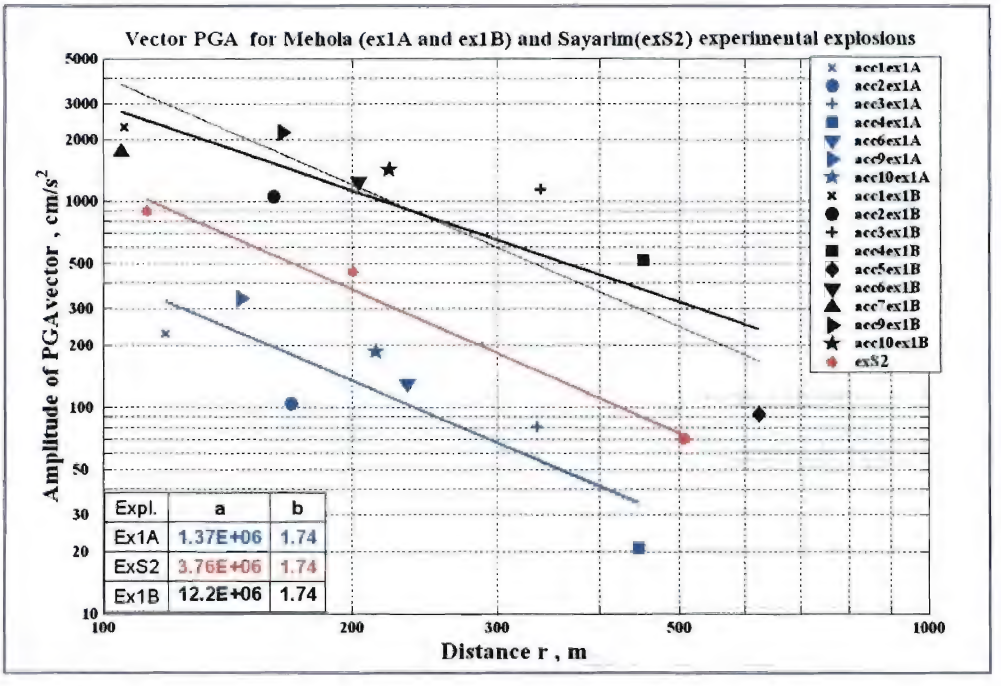

Figure 13. Vector attenuation with distance for experimental shots of similar charge weight.

Estimation of equivalent charge weight for Ex1A. If the power exponent is fixed as ***b=-1.74***, then using Equation 5, the charge scaling relation can be derived:

$$\mathbf{PGA \sim W^{0.58}} \quad (6)$$

Based on Equation 6 and using different pairs of explosions from Table 5 we evaluated a possible charge equivalent for Ex1A.

Table 5. Scaling coefficients for the three explosions and Exp1A charge estimation.

Explosion	Charge	Scaling coefficient a_i	Hole conditions
Ex1A	Unknown W_A	a_A=1.368 E+06	water on the bottom
ExS2	W_S=2000 kg (ANFO)	a_S=3.760 E+06	dry
Ex1B	W_B=3000 kg (Henamit)	a_B=12.21 E+06	full of water

1) for the pair (Ex1A,ExS2): $a_A/a_S = (W_A/W_S)^{0.58}$, then $W_A=2000*(1.37/3.76)^{1/0.58}$ =350 kg; possibly, an overestimated value, due to different (wet/dry) hole conditions (Table 5);
2) for the pair (Ex1A, Ex1B): $a_A/a_B =(W_A/W_B)^{0.58}$, then $W_A=3000*(1.37/12.21)^{1/0.58}$ =70 kg, possibly, an underestimated value due to water in the Ex1B hole, thus amplifying the seismic effect. If the amplification is ~2 times (W_B=6.1 instead of 12.2), then W_A~230 kg.
Finally we estimate the possible charge equivalent exploded in Ex1A as W_A~200-300 kg.
Another charge estimation based on strong-motion data is obtained from application of the Spectral Ratio procedure (see more details in Chapter 3.2.2) for the two explosions (Ex1A, Ex1B). The procedure applied to velocity spectra can also be applied to acceleration spectra. The ratios are flat at long periods with the relative amplitude indicative of a difference factor in source charge weight. We calculated spectra and the ratios for 1 sec P wave and 2 sec S wave time windows (Figure 14). In the low-frequency range 0.5-3 Hz both P and S spectral ratios are comparable and about flat with an average value ~10, providing an Ex1A equivalent charge size W_A~300 kg, similar to the previous estimates. Note a strong distinction in P and S spectral ratios at higher frequencies (3-40 Hz), showing a lower S-wave energy excitation for Ex1B in the higher spectral range compared to Ex1A.

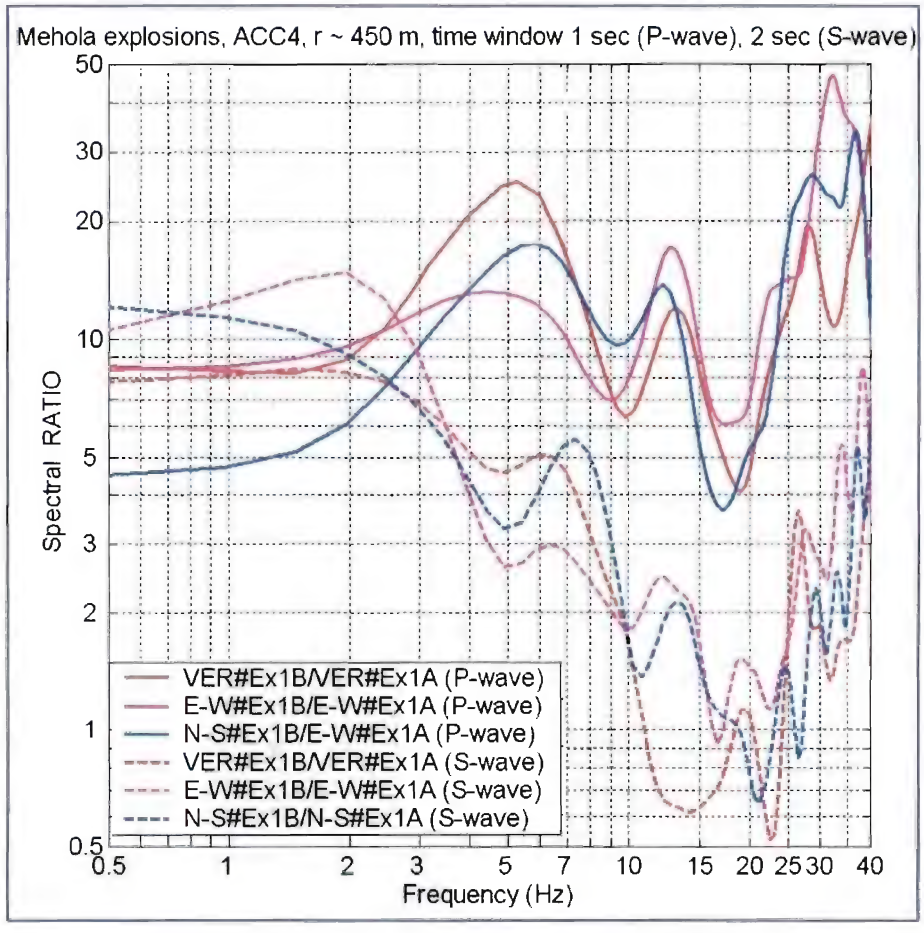

Figure 14. Spectral ratios of the two Mehola shots for different wave phases observed at remote accelerometer acc4 (r~450 m).

3.1.3. Seismograms at close distances

During the Mehola experiment three 3-component SP seismic stations (L4C seismometers) were deployed at distances of 3-10 km (see Figure 4) to the North. The seismograms, like the accelerograms, show much greater seismic energy for Ex1B than for Ex1A (Figure 15). P-waves are dominant on seismograms for both explosions, no clear S-wave and surface wave groups can be observed.

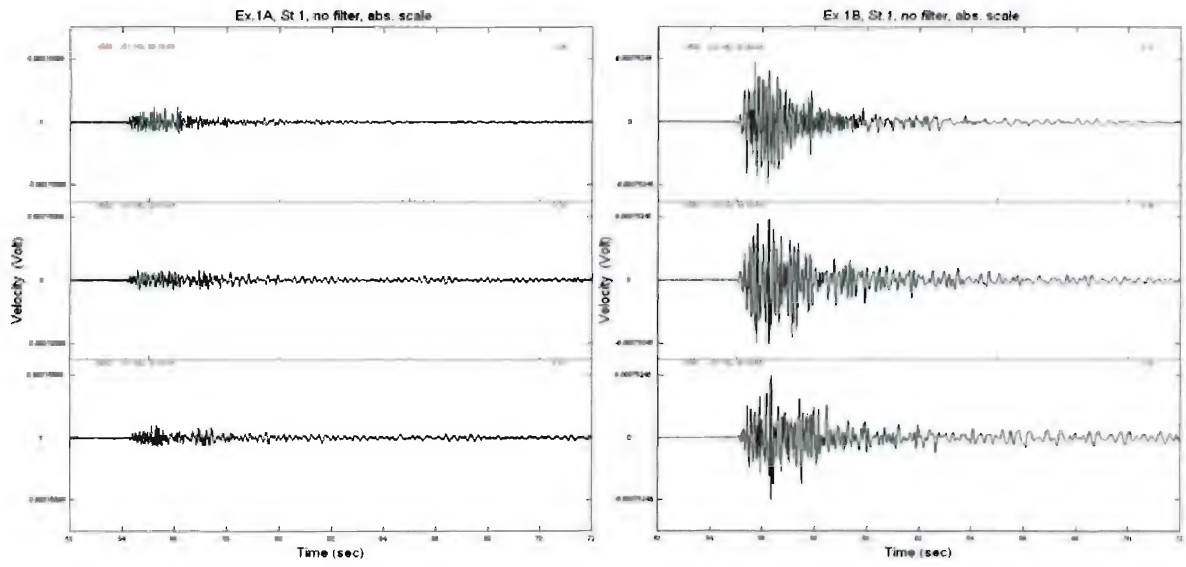

Figure 15. Seismograms of the Mehola explosions at 3-C portable station #1 (r~3 km). Note that scales for left (Ex1A) and right (Ex1B) plots are different.

Spectral analysis for Station #3 shows a concentration of seismic energy at 7-10 Hz for the weak shot Ex1A, compared to a lower frequency range of 4-7 Hz for the strong explosion Ex1B, also indicative of different source size (Figure 16).

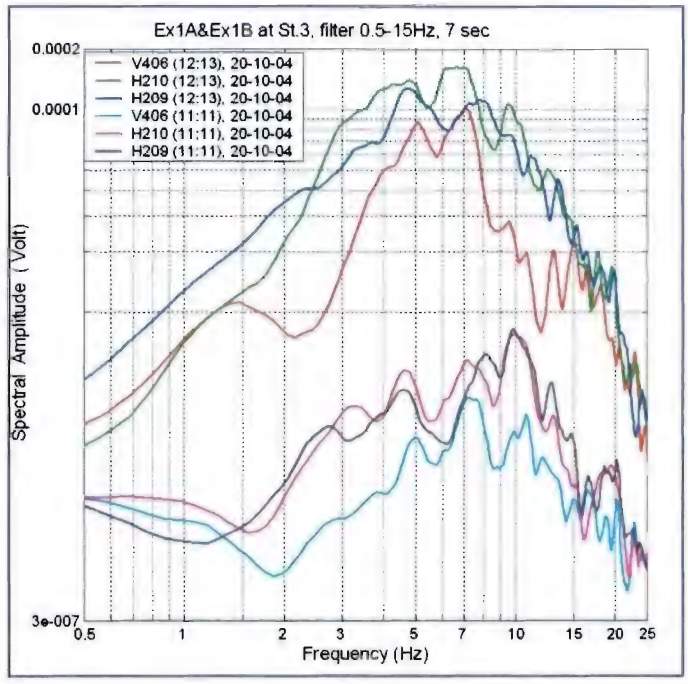

Figure 16. Spectra of Mehola shots at portable Station #3 (r~10 km).

3.2. Network SP and BB stations

3.2.1. Analysis of waveforms and manifestation of different regional phases

Clear Pn and Pg regional wave phases are observed from the large Sayarim explosion ExS3 at most elements of the remote IMS array AS049 at Mt. Meron at distance ~ 350 km (Figure 17).

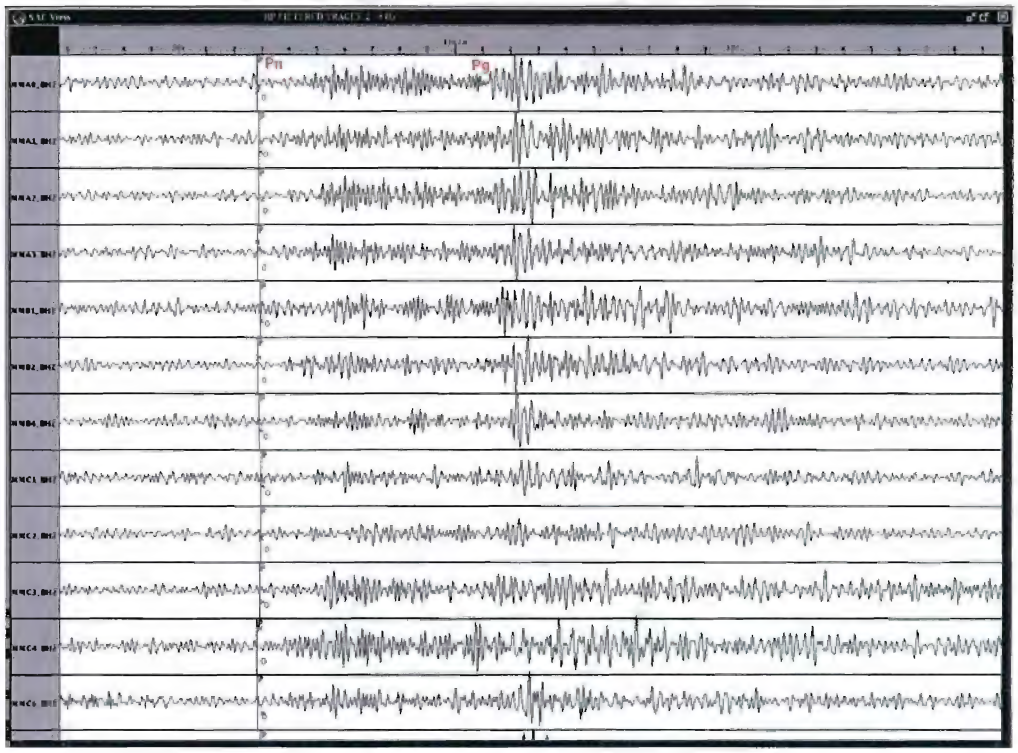

Figure 17. Seismogram of the large 32.5 ton shot recorded by the IMS array AS049.

Distinctive S-wave waveforms and S/P amplitude ratios were observed at network vertical SP stations from two experimental explosions of similar design (1 ton in a single hole) in Jordan (Ex.7) and Israel (Ex.9) conducted in the MERC project (see Figure 18). The Jordanian shot produced strong amplitude, dominant, P-waves and significant surface wave energy (at some close stations), but a clear S-phase was not observed. The Israeli explosion showed considerable S-waves and S-coda amplitudes and energy, and unexpectedly weak P-waves. The differences between the Jordan and Israel explosion recordings can be related to different geological settings in the near-source area, location in diverse tectonic units separated by the Dead Sea Transform zone, and some different features of the explosion design (Table 3).

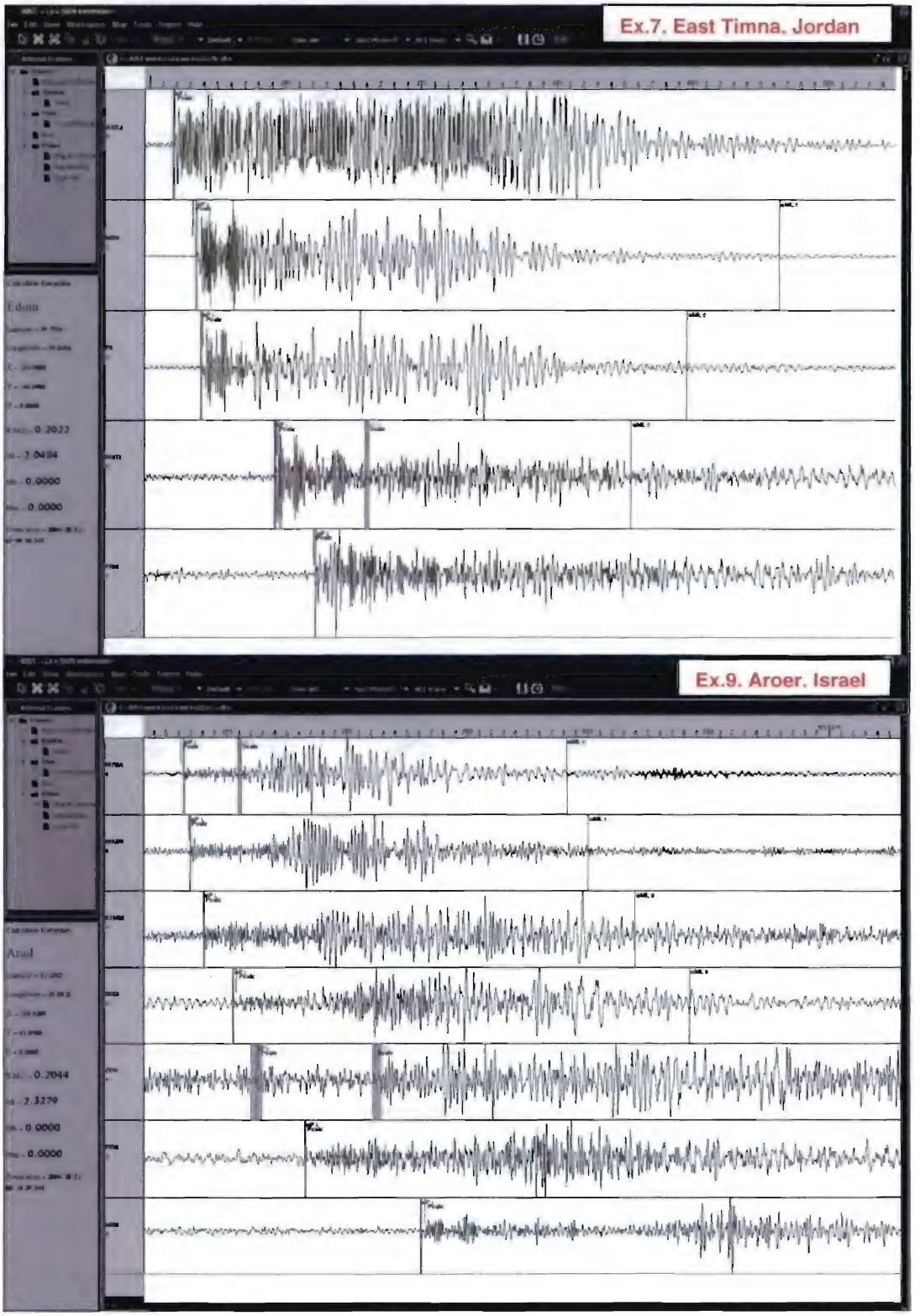

Figure 18. Sample of distinct S-waves for two explosions of similar design (charge 1 ton in a single hole), observed at ISN stations (vertical components).

An earthquake in the Arava valley (Q1) was collected in the project database due to its close proximity (~ 6 km) to one of the single experimental explosion (Ex6) (Table 3); both events are located in the Dead Sea Transform zone (see the event map in Figure 1). Strong dominant P-waves are found in the explosion seismograms for all vertical components at the distance range 31-163 km, whereas S-phases are not observed even on horizontal channels (PRNE, PRNN). Quite different regional phases are manifested at seismograms of the same stations for the earthquake: strong S-waves with clear onsets, weak P-waves resulting in high S/P ratio up to 10 and greater at the remotest MZDA station (124 km) (see Figure 19).

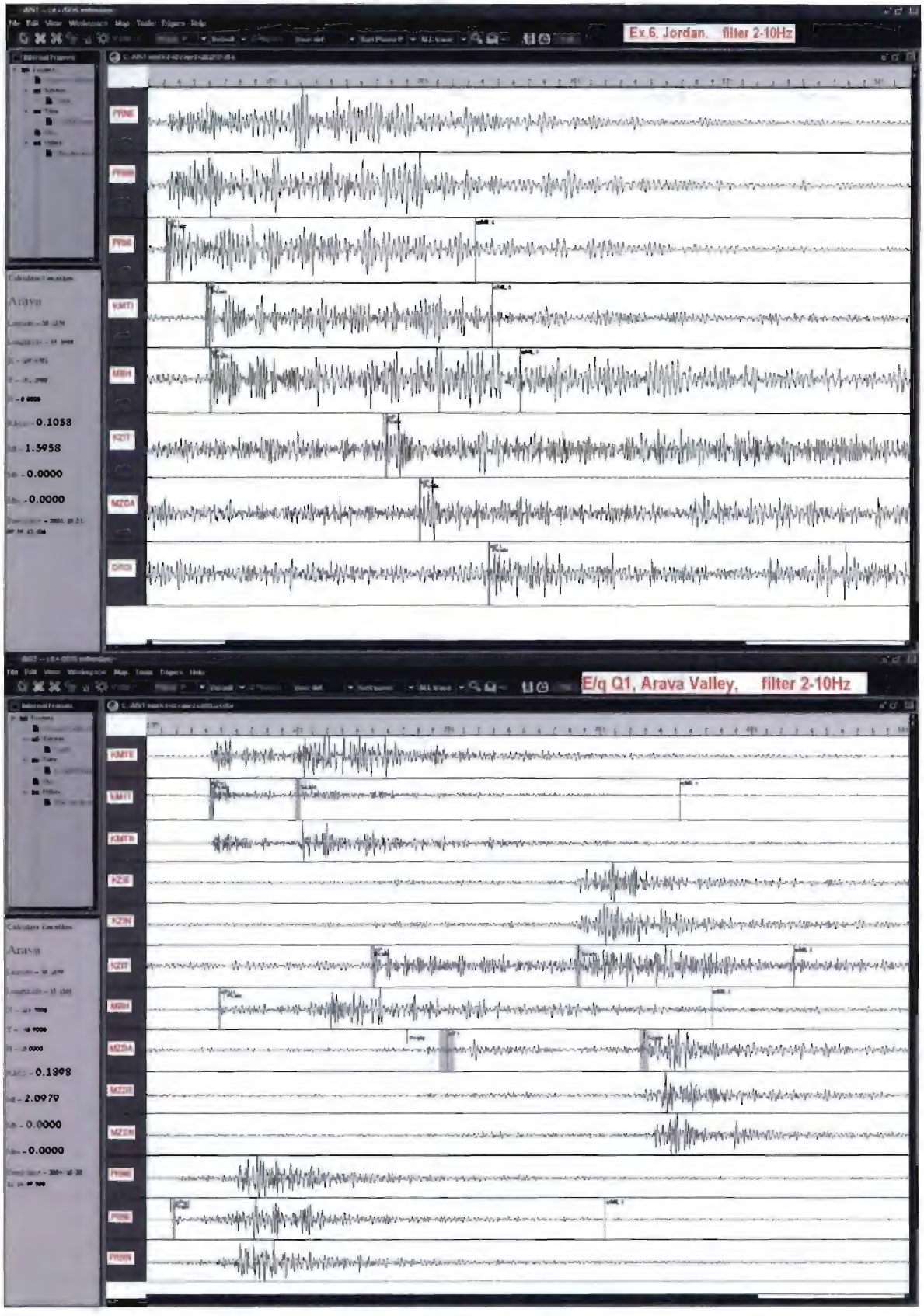

Figure 19. Different S-wave manifestation for an explosion and an earthquake located close to each other (~6 km) in the Dead Sea Transform zone.

3.2.2. Source Scaling estimations.

Spectral Ratio procedure. A simple procedure for estimation of the source function and corner frequency is provided by spectral ratios for specific single-fired explosions. The procedure scheme (based mainly on Stump et al., 2003) is presented on Figure 20. Amplitude spectra of velocity records on different components and selected time windows are used, to estimate source variations for regional waveforms.

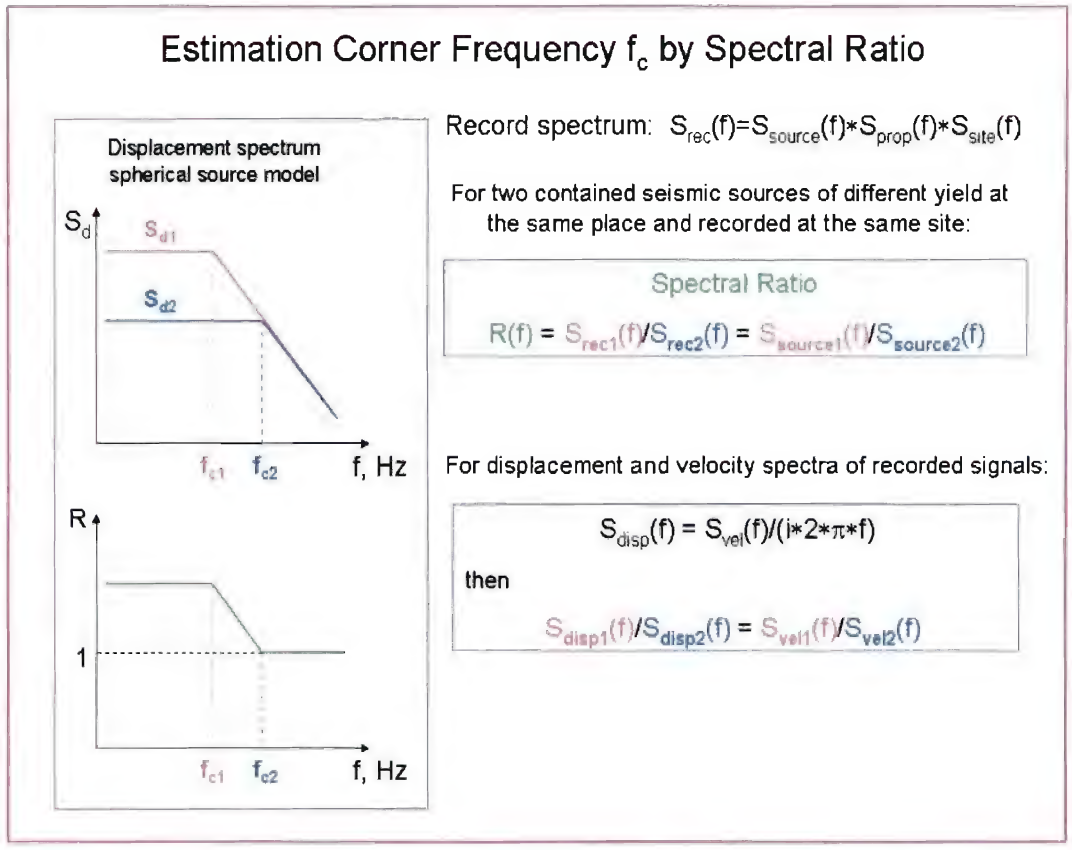

Figure 20. Illustration of the procedure using spectral ratios for estimating corner frequency of single-fired explosions.

The procedure was first applied to smoothed amplitude spectra of P and S waveforms to calculate spectral ratios and estimate corner frequencies for the pair of experimental Cyprus explosions, conducted for our previous project DTRA01-00-C-0119, and recorded at BB station CSS (see Gitterman et al, 2004). The explosions of 0.3 ton and 2 tons were ideally placed in the same point (the same deep borehole in a diabase rock massif, filled with water), providing an

identical propagation path; the observations are presented in Figure 21. Strong very high-frequency seismic signals with prominent dominant first P- arrivals are similar for both explosions; waveforms, spectral shapes and peak frequencies did not change for the larger shot, as expected from theoretical considerations, only amplitudes were increased (4-5 times) as expected. We suppose that the system "dynamite charge in deep borehole filled with water + strong hard rock diabase massif" behaved like a resonator tuned to a specific high frequency, not depending on the power of excitation).

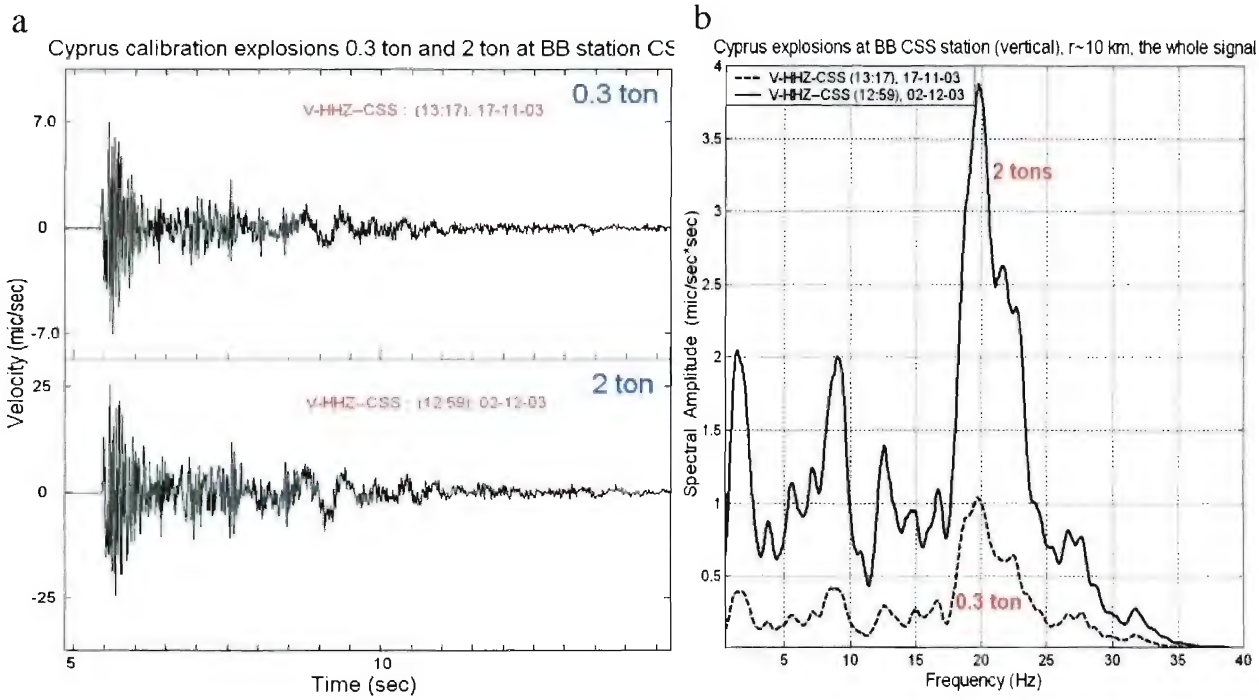

Figure 21. Seismograms (relative scale) recorded at CSS station (80 sps, r~10 km) for the pair of Cyprus shots (a), and smoothed spectra of the whole signal (8 sec) (b).

S-waves are not manifested clearly on the records; they are picked at ~1.3 sec after the P-wave arrival from the local velocity model, where an increase of waveform periods is observed on the E-W (about radial) and Z (Vert) components (see Figure 22, a). Low-frequency small-amplitude surface (Rg) waves are also present.

For calculation of spectra and spectral ratios for different regional phases we used time intervals of 1.3 sec for P and S waves and 4 sec for Rg (surface) waves. Comparison of spectra for the vertical component, presented in Figures 21 and 22, shows that most of the seismic signal energy for both explosions is focused in very high-frequency maximum amplitude P-waves at 18-

23 Hz, a smaller part of the P-energy is in a middle-frequency range of 8-10 Hz; the energy of S-waves is concentrated in the same spectral ranges, but lower by factor of ~10. The energy of Rg waves is found in the 1-2.5 Hz interval.

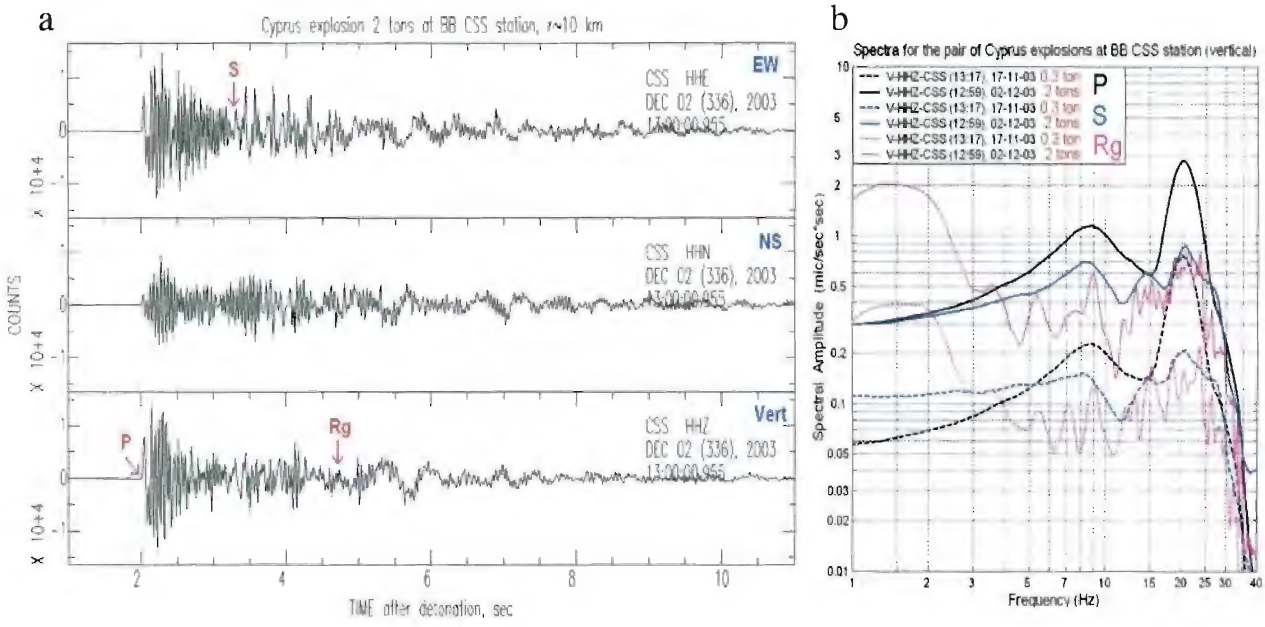

Figure 22. 3C seismogram of the large Cyprus explosion at CSS station (a); smoothed spectra of different phases on the vertical component for both explosions (b).

Smoothed amplitude spectra of P, S and Rg (surface) waves were used to calculate spectral ratios on different components and estimate corner frequencies for the Cyprus explosions (Figure 23). Spectral ratios for both P and S waveforms give similar estimates of the source differences at all frequencies for the EW component (Figure 23, b), and in the range 10-30 Hz for the vertical component (Figure 23, a). The P, S ratios are about flat at low frequencies, with the relative amplitude ~5 corresponding to the factor of 6.5 difference in source charge weight (for the vertical S-waves the low-frequency part is not flat and is underestimated). The corner frequency of the larger explosion is about 10 Hz where the ratio begins to decrease to the lower plateau at ~25-28 Hz, the corner frequency of the smaller explosion. The Rg ratio shows a large variability (Figure 23, f), and similarity to the body wave ratios on the vertical and EW components (Figure 23, a, b). The NS component shows variable ratio curves, inconsistent with other components.

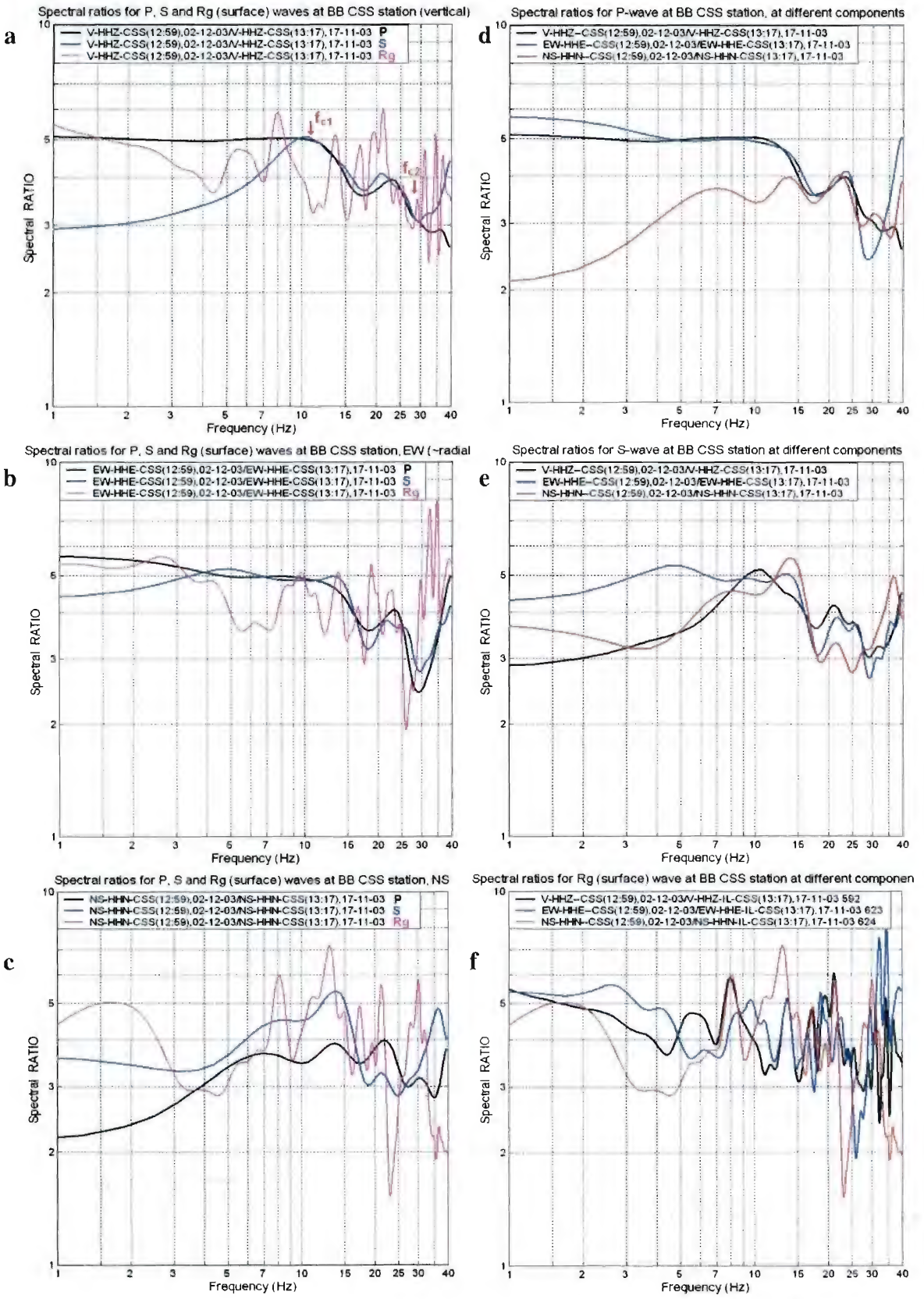

Figure 23. Spectral ratios for different wave phases on 3 components of BB station CSS.

Final corner frequency estimations for the large (f_{c1}~11 Hz) and small (f_{c2}~28 Hz) explosions were found. The results obtained, jointly with estimates for almost-contained blasts in a mine in Wyoming, recorded at the Pinedale array (Stump et al., 2003), were used for computation of an empirical corner frequency-yield relation (7).

The Cyprus explosions can undoubtedly be considered as fully contained despite impressive external effects. Both datasets showed consistency in spite of different conditions (charge design, scaled depth, geological settings, distances), resulting in a well-fit regression curve (Figure 24):

$$f_c = 266*W^{-0.4161} \qquad (7)$$

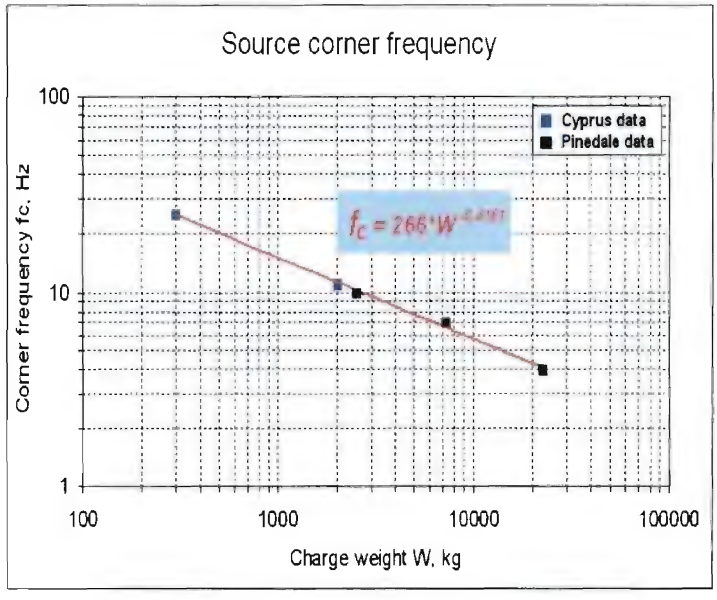

Figure 24. Empirical corner frequency-yield relation based on data from single-fired contained explosions in Cyprus and Wyoming.

A similar spectral ratio analysis was carried out for the pair of Mehola explosions, conducted in October 2004 (see Chapter 1.1.2, Table 3). Near-source seismic data were used to investigate the characteristics of the anomalous single-fired shot Ex1A that produced small amplitudes (as presented before, see Figure 15), and estimate a detonated charge equivalent, similar to the analysis of two partially detonating shots in the Wyoming experiment (Stump et al., 2003).

Spectral ratios using the portable three-component short-period seismic station #1 in the near-source area for this shot compared with the fully detonated Ex1B are presented in Figure 25.

The station was deployed at ~3 km to the North from the explosions, the data were sampled at 100 sps, and a band-pass filter 0.2-25 Hz was included in the recording system. Another spectral ratio estimation using data of the closest short-period network station HMDT (vertical) at 4.4 km is shown in Figure 26. These spectral ratios suggest that Ex1A was reduced by a factor of ~20 in average for the flat ratio function part in the low-frequency range, resulting in the detonated charge equivalent W~150 kg (3000 kg/20), which is similar to other estimates from near-source strong motion observations (see Chapter 3.1.2).

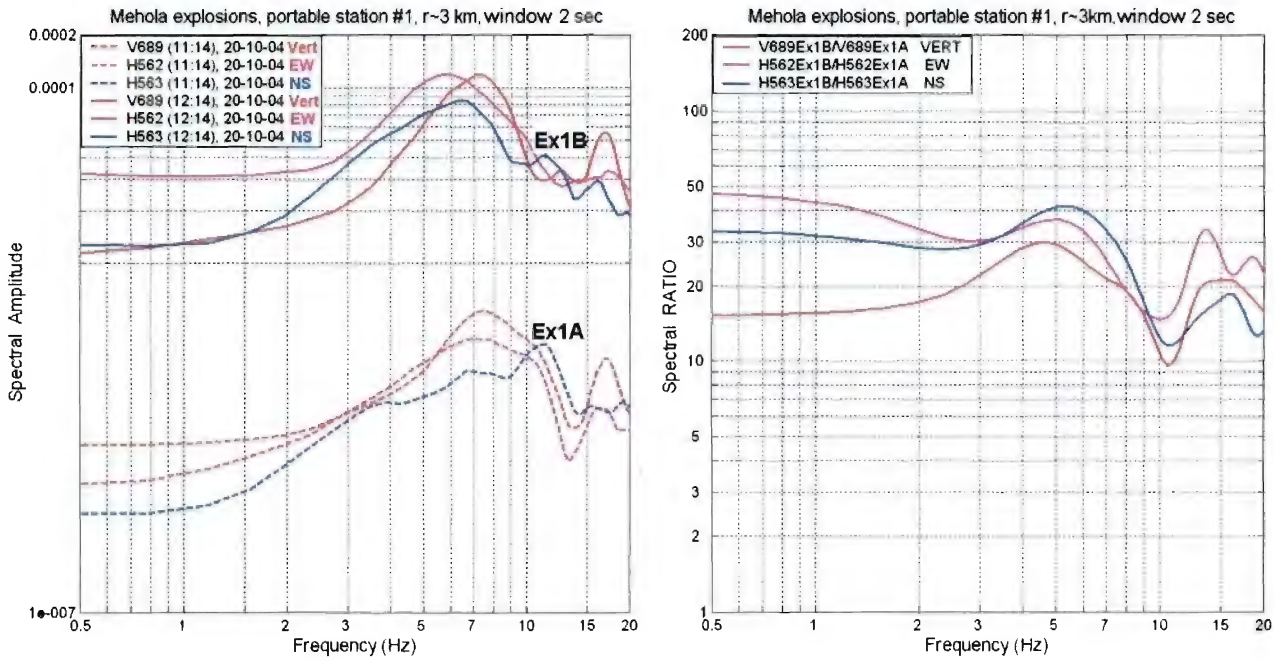

Figure 25. Spectral ratio for the two Mehola shots at portable station St.1 (EW - about transversal). A time window of 2 sec was used, including P and S waves.

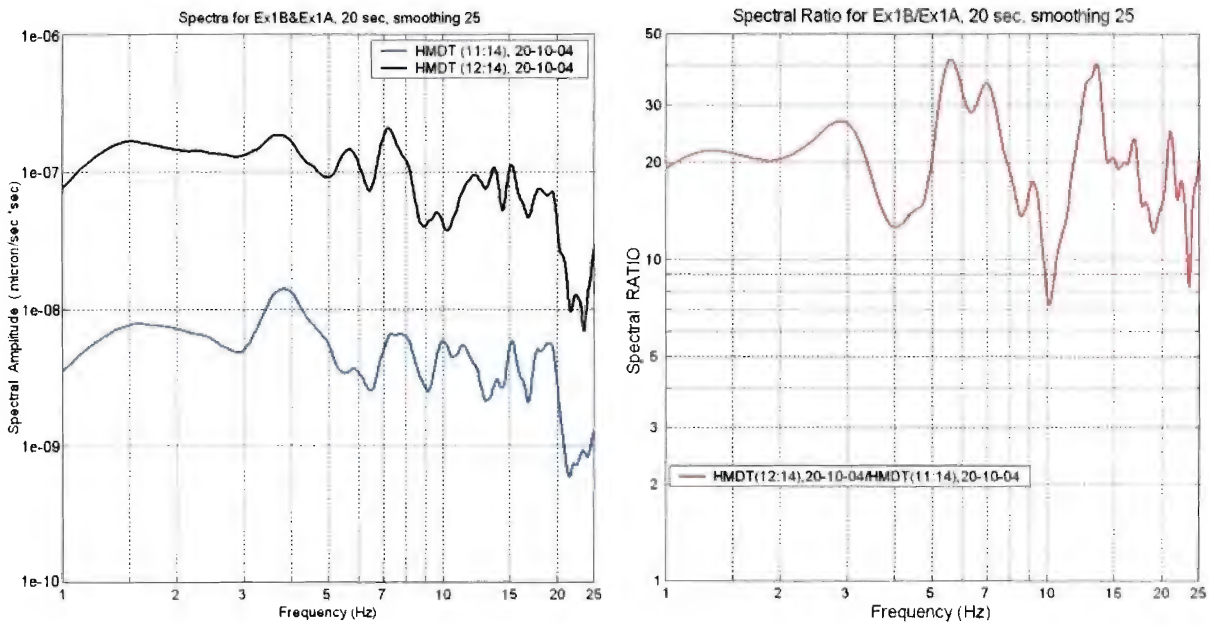

Figure 26. Spectral ratio for the two Mehola shots on the vertical component of ISN station HMDT. A time window of 20 sec was used, including the whole signal.

An observed decrease of the spectral ratios at ~7-8 Hz can be related to the estimated corner frequency for the strong shot Ex1B of 3 tons, that is close to the value fc~9 Hz from Equation (7). Filter upper limits on recording channels (12 Hz at ISN network stations, and 25 Hz at the portable station) prevented possible observation of a corner frequency ~30-35 Hz for the partially detonated charge of Ex1A.

Peak Amplitude scaling. All three experimental explosions of the Sayarim charge-weight series were well observed at the IMS BB station EIL (Figure 27). Inspection of observed waveforms on the 3C record (Figure 28) identifies regional phases P, S and Rg (surface waves).

Vertical Peak Amplitudes (VPA, micron/sec) were measured for each of the phases and plotted against charge weight for shots S1-S3 in Figure 29. TNT equivalent charges were used (Table 2) and for the multiple-hole explosion S3 the total charge was taken.

The data for each phase are fit with the power low equation:

$$VPA_{(mic/sec)} = A * W_{(kg)}^{B} \qquad (8)$$

An r.m.s. procedure produced estimates of ***A*** and ***B*** for each of phases P, S and Rg (Table 6).

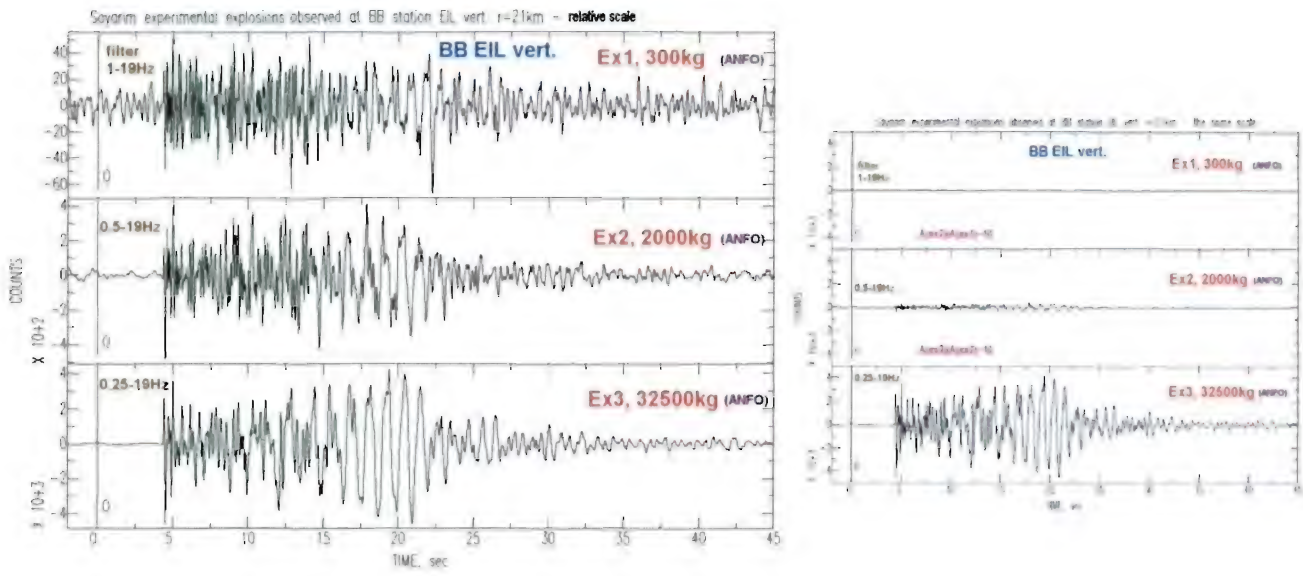

Figure 27. Seismograms of Sayarim explosions at EIL (vertical) in relative (left) and absolute (right) scale.

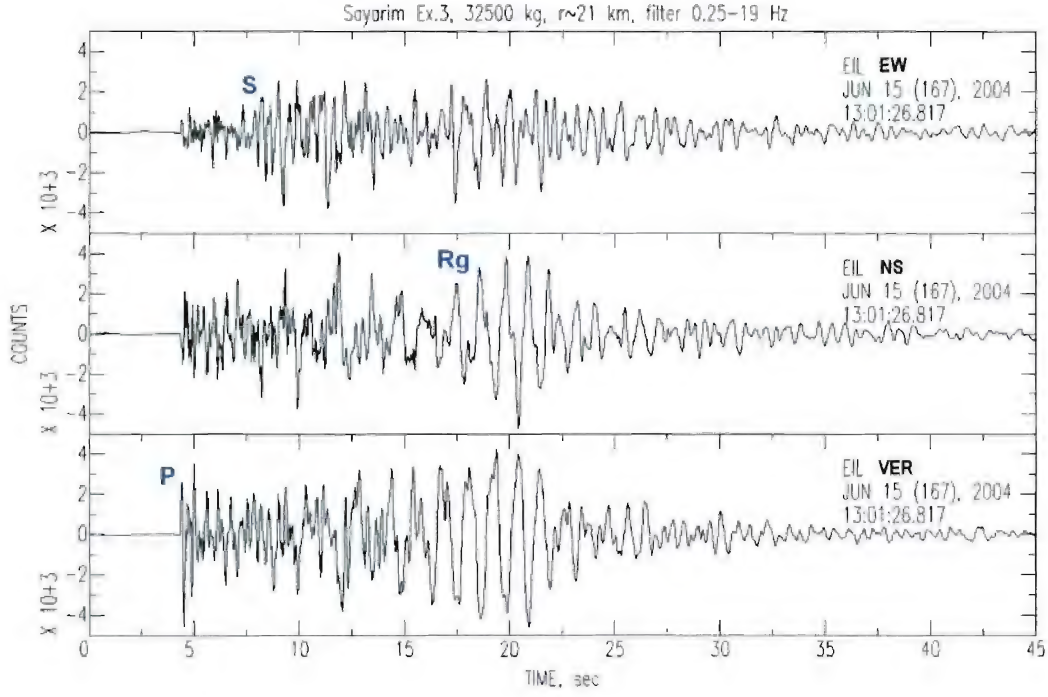

Figure 28. 3C seismogram at EIL BB station of the largest Sayarim Ex.S3. Three regional phases can be identified.

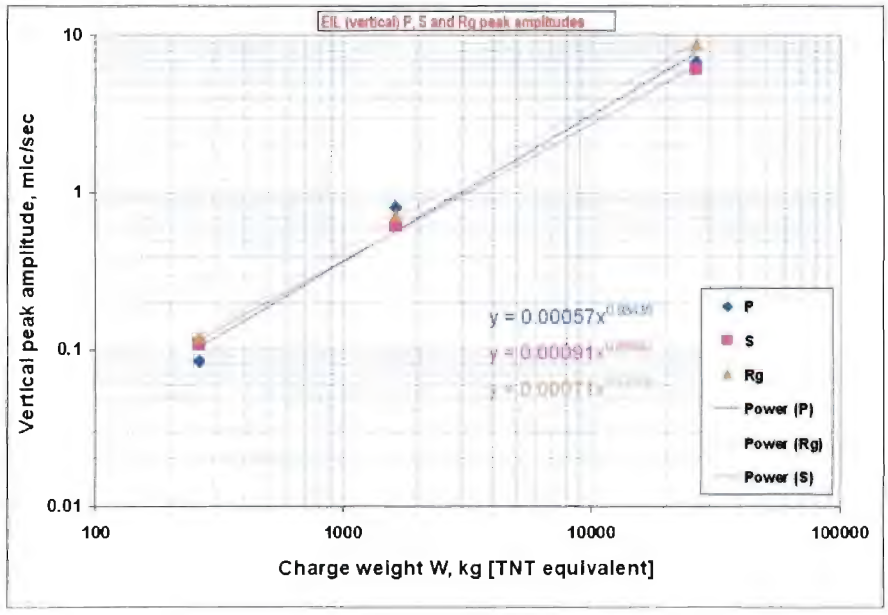

Figure 29. Peak amplitude (vertical component) source scaling for different wave at local distances.

Table 6. Estimated source scaling parameters in Equation (8).

Phase	B	A
P	0.934	5.7E-04
S	0.870	9.1E-04
Rg	0.928	7.1E-04

Power law fits to each phase demonstrate little difference between the source yield scaling parameter ***B*** (0.87-0.93) for the different phases. The ***B***-values obtained are in close agreement with the scaling parameters of Vergino and Mensing (1983) for Pn waves from nuclear explosions in Nevada, and of Stump et al. (2003) for Pn, Pg, and Lg regional phases (0.84-0.91) from chemical explosions in Wyoming. The ***A*** value depends on distance and site conditions and for the station considered (EIL) is comparable for all three phases, similar to estimations of Stump et al. (2003) for Pg and Lg phases.

3.2.3. S/P maximum amplitude ratios in different frequency bands

Different kinds of amplitude and spectral ratios for different wave phases are used for discrimination purposes (see e.g. review of Blandford, 1995, and more recent research of Walter et al., 2004). We analyzed the S/P maximum amplitude ratio in different frequency bands, using the software developed (see Chapter 2.2.1). For this case study we used four explosions in the Sayarim area. Seismograms at ISN vertical stations were filtered in three spectral bands: 0.5-3 Hz (low filter), 3-6 Hz (medium filter) and 6-9 Hz (high filter), and maximum amplitudes were measured in windows 3-5 sec after P and S arrivals (Figure 30). A wide filter (0.5-12 Hz) including the whole recording frequency range was also used in the analysis.

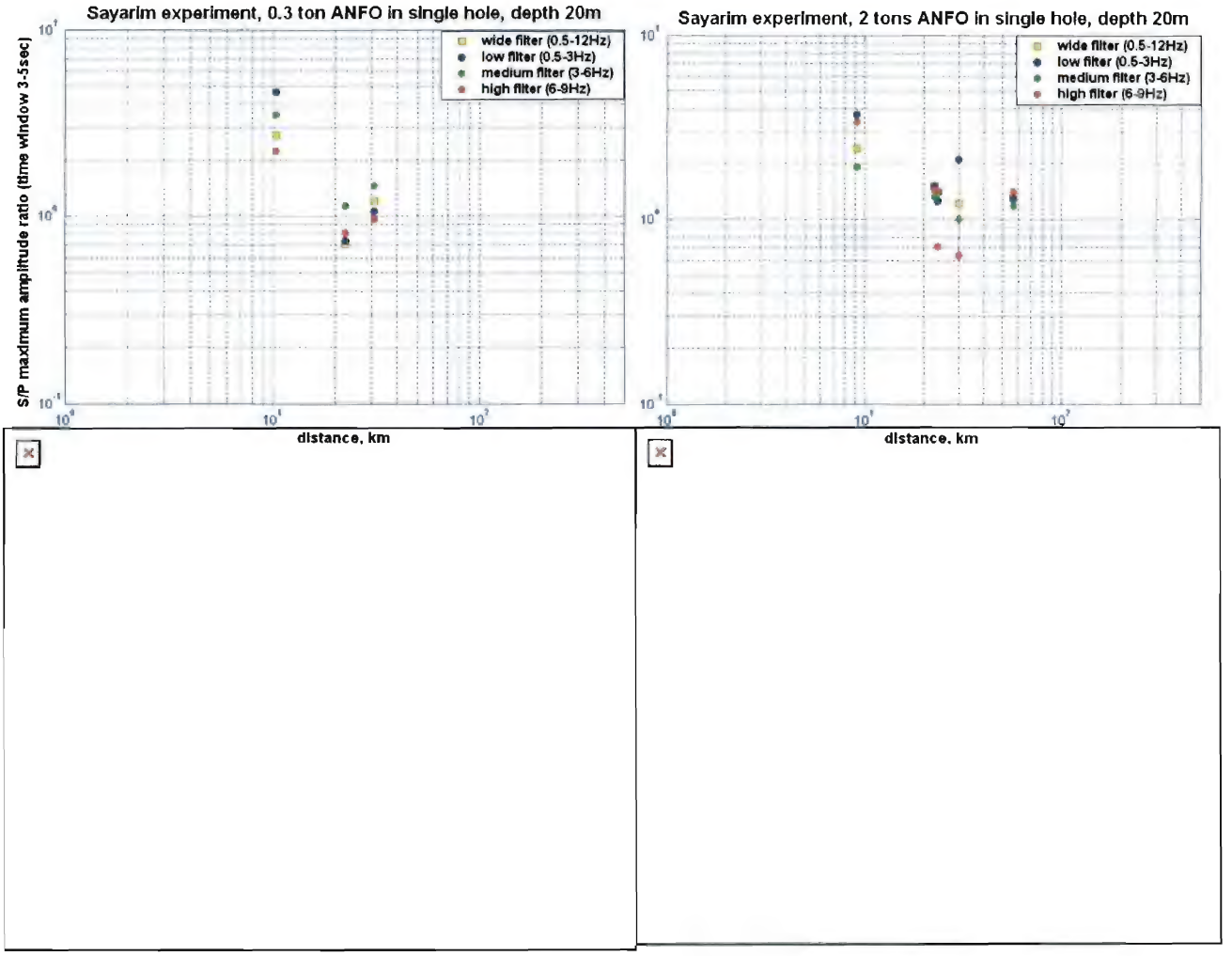

Figure 30. S/P maximum amplitude ratios vs distance for observations at different SP ISN stations from single-fired explosions in the Sayarim area.

S/P maximum amplitude ratios obtained for different ISN stations, presented in Figure 30, do not manifest clear dependences on distance and frequency band.

If the ratio values for a fixed shot are averaged over the stations, then two tendencies can be observed: a decrease with charge (especially for low and medium filters) and higher ratios for the lower frequency band (Figure 31).

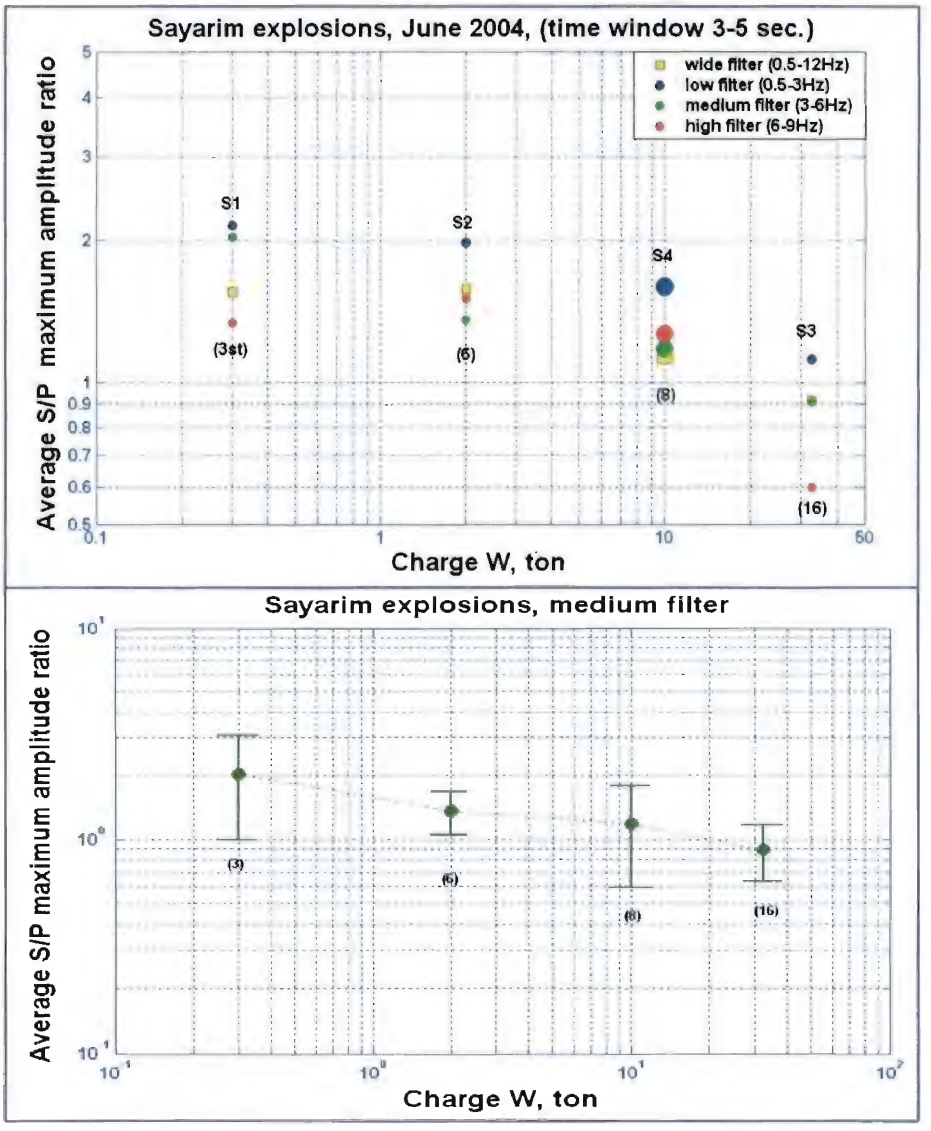

Figure 31. S/P maximum amplitude ratios vs charge averaged for different ISN stations for Sayarim explosions (top); mean and standard deviation estimations for the medium filter (3-6Hz) (bottom). Number of processing stations (n) is also shown.

Note that the explosion S4 of 10 tons TNT on surface is consistent with three other borehole ANFO shots located in the same area.

This S/P parameter shows potential for identification of explosion seismic sources and discrimination between earthquakes and explosions, and will be tested on other explosions and earthquakes.

3.2.4. Estimating energy partitioning for observed phases.

For this case study we took the large (32.5 tons) explosion ExS3 in the charge-weight experimental series in Sayarim valley (see Table 1) and applied the processing procedure developed (see Chapter 2.2.2). As a first stage we choose to analyze signals in a broad frequency range, with the filter (0.5-12 Hz) applied to the records. Considering the recording range for short-period stations, and the observed frequencies for local distances and magnitudes analyzed, it is reasonable to say that seismic energy was calculated for unfiltered signals.

The analysis was focused on four portions of the signal:

1) All the signal – 60 seconds from the P phase start;
2) P-waves – 2 seconds since P arrival,
3) S-waves – 2 seconds since S arrival,
4) Surface waves – starting 2.5 sec after S-arrival up to twice the S-arrival lapse time.

The P and S first arrivals are computed from the local 1D velocity model.
The seismic waveform energy was computed as the sum of squares of amplitudes over the specified time interval for two groups of data separately: 3C network short period and BB stations, and vertical component stations (see the map in Figure 1).

For the 3C stations amplitudes are the square root of the sum of component amplitudes (Equation 1). The results of computations for 6 3C stations are presented in Figures 32, 33. The stations range from 21 km (EIL) up to 187 km (AMZI). Energy partitioning for the stations are shown in Figure 33 as percent of the total energy computed in the [P arrival, P+60 sec] time interval. The estimates show that the energy in 3C motion in the S time interval is dominant relative to the P time interval and varies within 10%. The surface waves accommodate most of the signal energy, and increase with distance.

Energy of P waves for vertical channels is dominant over S wave energy (Figure 34). Surface waves annex almost all the seismic energy of the signal at larger distances. The stations used in the analysis range from 7.8 to 388 km. Energy partitioning is shown in Figure 35.

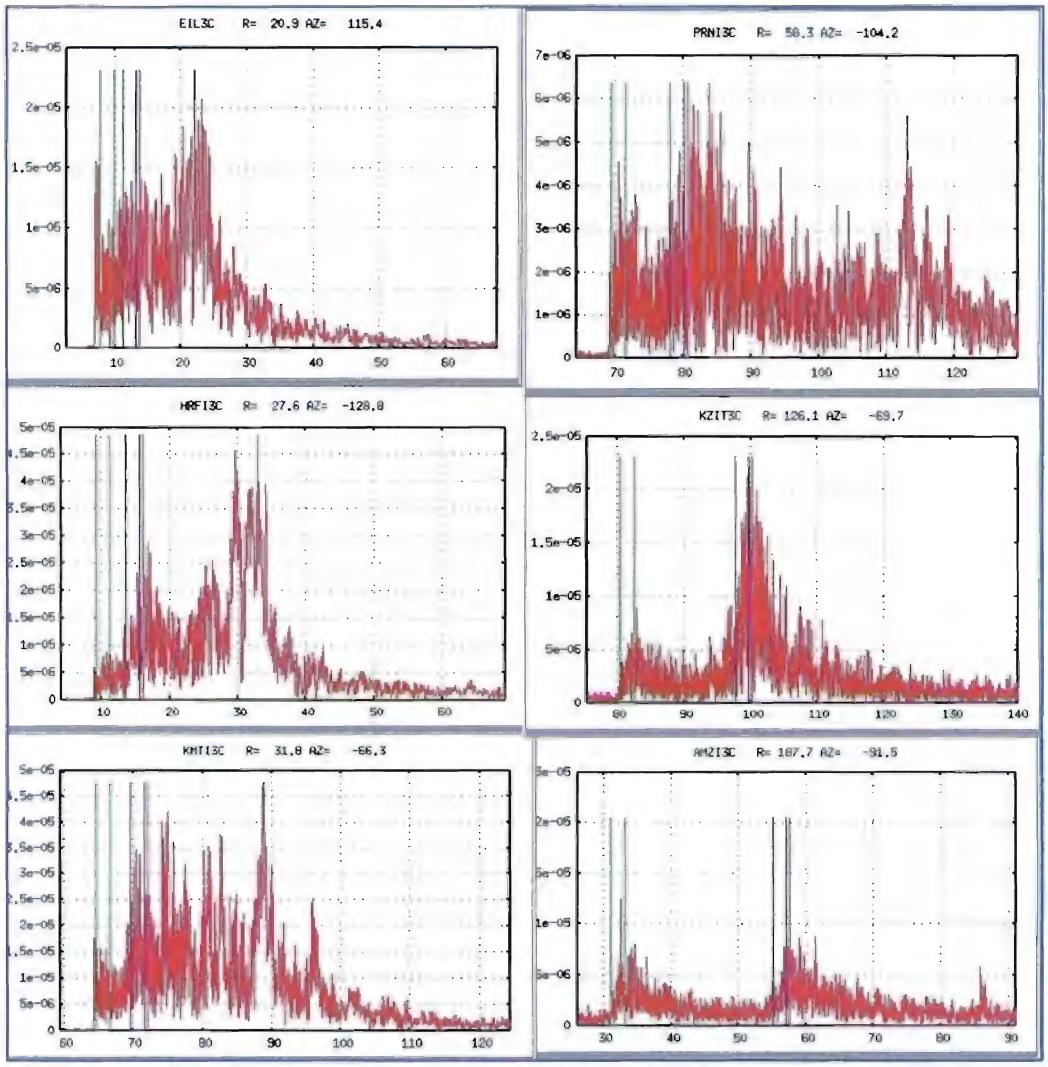

Figure 32. Amplitudes (m/sec) versus time (sec) for six 3C stations (3 BB and 3 SP stations) (shot ExS3). Vertical lines mark time intervals for energy computation.

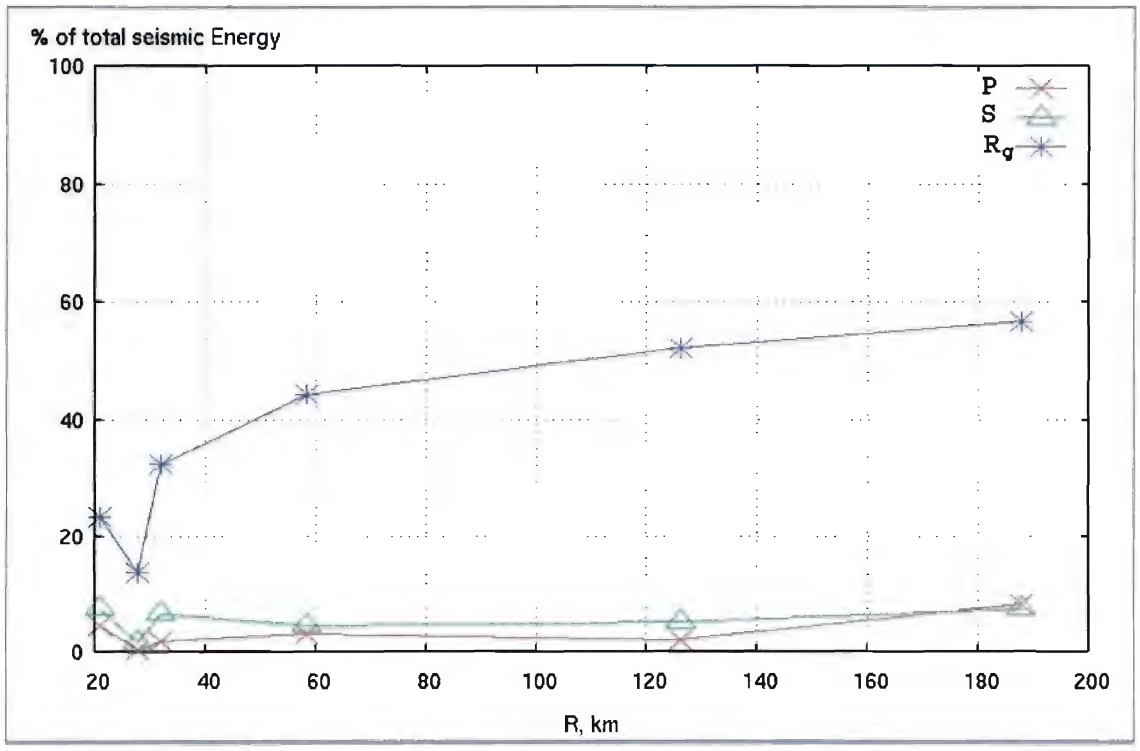

Figure 33. Energy partitioning between P, S and Rg (surface waves) for the six 3C stations as computed in the time intervals, shown in Figure 32 (shot ExS3).

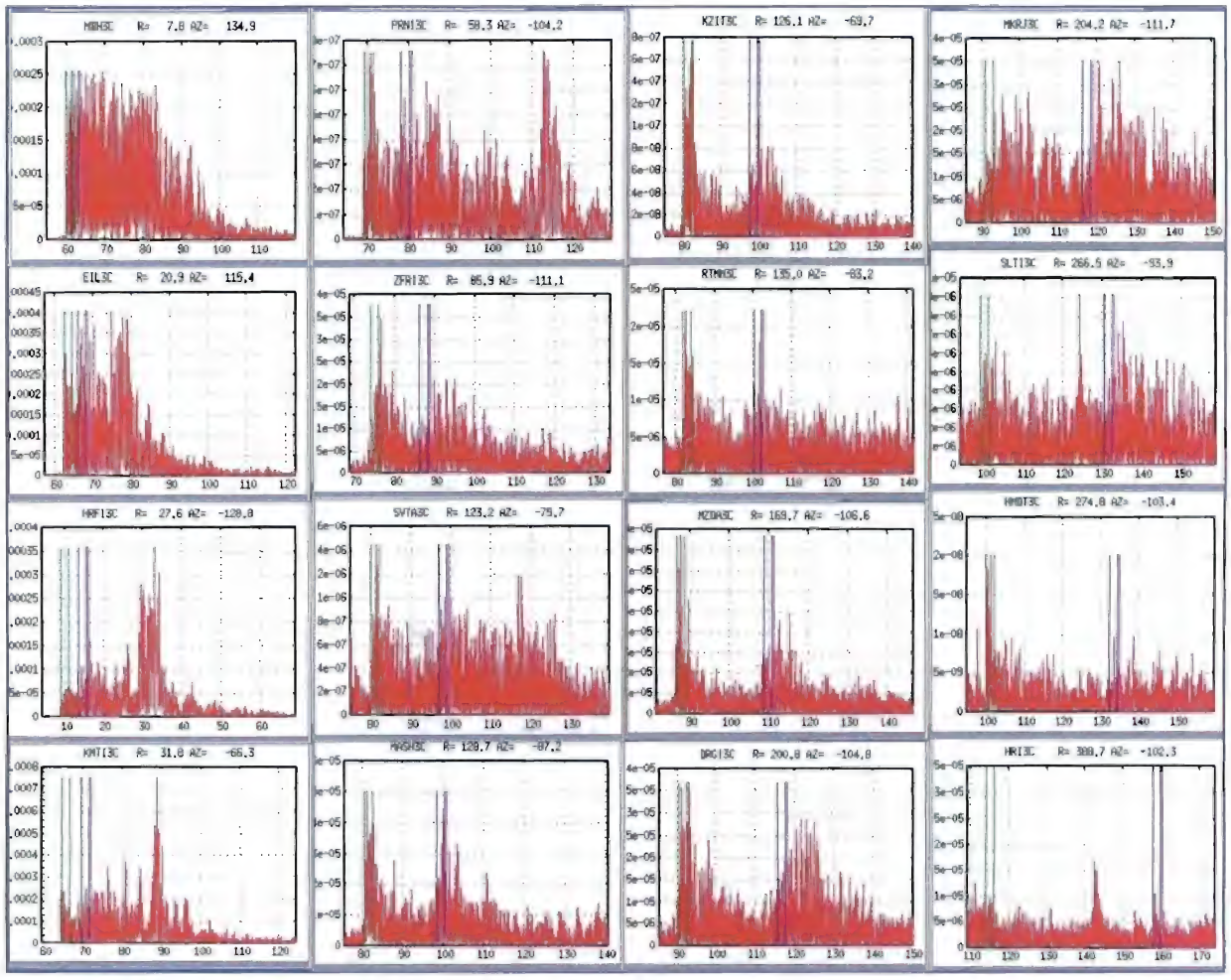

Figure 34. Amplitudes (m/sec) versus time (sec) for sixteen vertical channels of the BB and SP stations (explosion ExS3). Vertical lines indicate time intervals for energy computation.

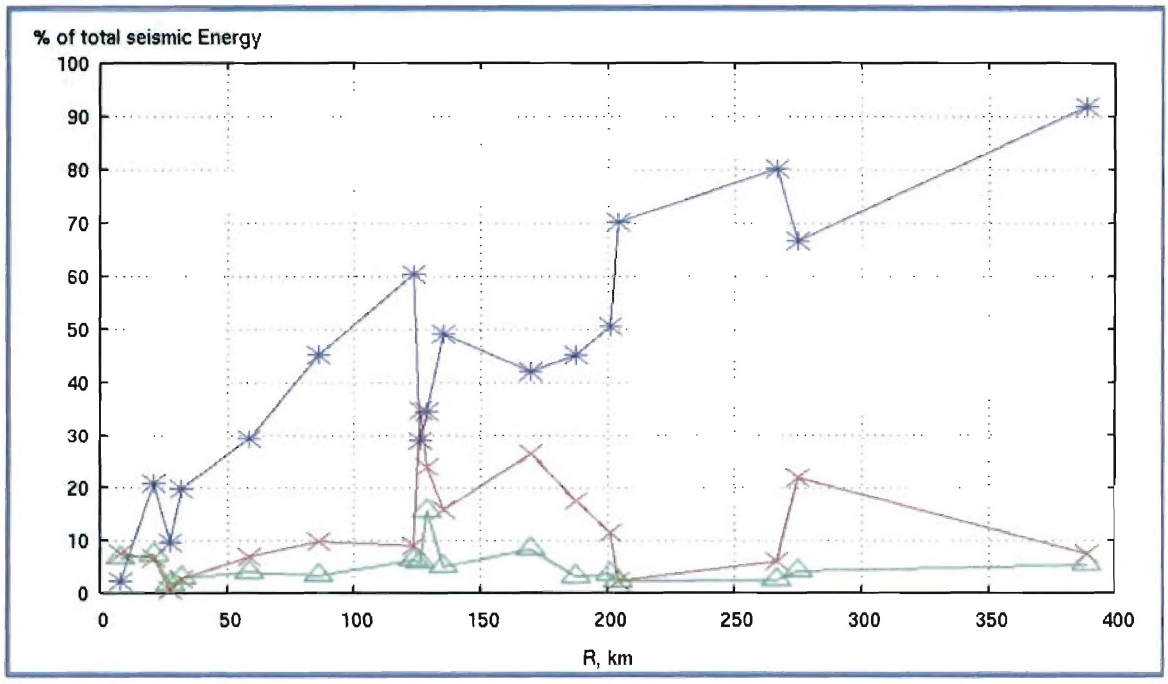

Figure 35. Energy partitioning between P, S and Rg (surface waves) for sixteen 3C vertical stations as computed in the time intervals, shown in Figure 34 (shot ExS3).

4. CONCLUSIONS

The project event database was created to study empirical features of seismic energy generation for different seismic sources (especially for S waves from explosions), and how this energy is partitioned between P and S waves. Explosions selected present a broad variety of design features, charge weight, burial depth, emplacement rocks and geological settings.
A number of experimental single-fired explosions were conducted and numerous 3C and vertical observations were acquired from the near-source zone (0.1 km, by accelerometers) to near-regional distances (390 km, by seismic stations of local networks in Israel and Jordan).
From regional observations of the Sayarim charge-weight series, significant seismic strength was achieved in spite of non-consolidated sediment media (dry alluvium, commonly considered as low-coupling material) and shallow burial depth that caused poorly contained explosions (gas and rocks blowout on the surface, and cratering).

GT parameters and local seismic stations records were collected for a number of large controlled quarry and military blasts. The events selected were recorded by SP and BB instruments, and seismic arrays, including IMS stations. Preliminary analysis showed a diversity of regional phase (P, S, Rg [Lg]) manifestation.

To fulfill project goals existing software was modified and new programs and scripts were developed. For case study analysis the computer procedures were applied to the Sayarim experimental explosion series of variable charge weight. Preliminary results show some tendencies in dependency of S/P maximum amplitude and energy ratios on distance and yield. Source scaling estimations based on BB records at local distances of the same series show similar yield scaling parameters (0.87-0.93) for different regional phases. The power law parameter values (approximately linear increase in peak amplitude with explosive weight) are in close agreement with the constants for nuclear explosions in Nevada and chemical explosions in Wyoming.

Application of the spectral ratio procedure to data collected for some experimental explosions provided important estimates of the corner frequency-charge weight relation and the equivalent yield of a partially detonated explosion.

The analysis will be continued for other events from the dataset selected and new planned experimental shots to validate the results obtained.

5. REFERENCES

Blandford, R.R. (1995), Regional seismic event discrimination, in: E.S. Husebye and A.M. Dainty (eds.) a Comprehensive Test Ban Treaty, NATO ASI Series, Series E: Applied Sciences - Vol. 303, 689-719.

Gitterman, Y. (1998), Magnitude-yield correlation and amplitude attenuation of chemical explosions in the Middle East, Proceedings of the 20th Annual Seismic Research Symposium on Monitoring a CTBT, 302-311.

Gitterman, Y. and A. Shapira (2001), Dead Sea Seismic Calibration Experiment contributes to CTBT Monitoring, Seismological Research Letters, Vol. 72, Num. 2, March/April 2001, p. 159-170.

Gitterman, Y., V. Pinsky, A. Shapira, 2003. Improvements in Monitoring the CTBT in the Middle East by the Israel Seismic Network, Final Report, Rep. DTRA-TR-01-35, October 2003, 196 pp.

Gitterman, Y. and V. Pinsky (2004), Using Ground Truth Events for Travel Time Calibration and Studying Seismic Energy Generation and Partitioning into Various Regional Phases, AFRL Program Review 20 September 2004, Orlando, Florida.

Gitterman, Y., V. Pinsky, K. Solomi, R. Hofstetter, C. Gurbuz, and M. Ergin (2004). Using ground truth events for travel time calibration and studying seismic energy generation and partitioning into various regional phases, Proceedings of the 26th Seismic Research Review "Trends in Nuclear Seismic Monitoring", Orlando, Florida, September 21-23, 2004.

Kurpan J. (2004), Discrimination of seismic events in Israel recorded by national seismic network, M. Sc. Thesis, Tel-Aviv University, supervisors Prof. Z. Ben-Avraham and Dr. Y.Gitterman.

Negmatullaev S.Kh., M.I. Todorovska, M.D. Trifunac (1999), Simulation of strong earthquake motion by explosions – experiments at the Lyaur testing range in Tajikistan. Soil Dynamics and Earthquake Engineering 18 (1999), 189-207.

Stump, B., D.C. Pearson and V. Hsu (2003), Source scaling of contained chemical explosions as constrained by regional seismograms, Bull. Seism. Soc. Am. 93, 1212-1225.

ten-Brink, U., Al-Zoubi, A., Rybakov, M. and Rotstein Y. (2004), Integrated geophysical study of the Dead Sea rift for hazard assessment and mineral resources. MERC program of U.S. AID, Grant No. TA-MOU-01-M21-012.

U.S. Congress (1988), Office of Technology Assessment, Seismic Verification of Nuclear Testing Treaties, OTA-ISC-361 (Washington, DC: U.S. Government Printing Office, Chapter 6, May 1988).

Vergino, E.S., and R.W. Mensing (1983), Yield estimation using regional m_bP_n, Bull. Seism. Soc. Am. 80, 1200-1206.

Walter, W.R., K.M. Mayeda, A.J. Rodgers, S.R. Taylor, D.A. Dodge, E. Matzel and M.D. Ganzberger (2004), Regional Seismic Identification Research: Processing, Transportability and Source Models, Proceedings of the 26th Seismic Research Review "Trends in Nuclear Seismic Monitoring", Orlando, Florida, September 21-23, 2004.